

Article

Trend of Vegetation and Environmental Factors and Their Feedback in the Karst Regions of Southwestern China

Kai Huang ¹, Rui Wang ², Weixiong Wu ¹, Peilin Wu ¹, Haoxiang Li ^{3,*}, Linglin Zeng ^{3,*}, Jinhua Shao ¹, Haichen Liu ³ and Tao Xu ³

¹ Guangxi Key Laboratory of Water Engineering Materials and Structures, Guangxi Hydraulic Research Institute, Nanning 530023, China

² Changjiang Geotechnical Engineering Corporation, Changjiang Institute of Survey, Planning, Design and Research, 1863 Jiefang Street, Wuhan 430010, China

³ College of Resources and Environment, Huazhong Agricultural University, Wuhan 430070, China

* Correspondence: l_h_x@webmail.hzau.edu.cn (H.L.); zenglinglin@mail.hzau.edu.cn (L.Z.)

Abstract: Vegetation plays a vital role in the terrestrial ecosystem. Vegetation variations not only result from climatic and environmental change but also feed back to the climate through biogeochemical and biogeophysical processes. Previous studies have mainly focused on the influence of environmental factors on vegetation changes, but the interactions between vegetation and the prevalent environmental factors in the karst areas of southwestern China have been poorly understood. Based on remote sensing data, this study used trend analysis and Granger causality analysis to investigate vegetation trends, the driving factors, and their interactions during the period 2001 to 2021. In summary, we explored how these factors influenced vegetation growth and how vegetation changes fed back to produce ecosystems and environmental variations in southwestern China during this period. The results showed improvements in water conditions as well as a vegetation greening trend in most of the regions of southwestern China, together with a weakening trend of rocky desertification and an increasing trend of vegetation growth during the period. Both terrestrial water storage and vegetation growth in the energy-limited alpine regions are sensitive to temperature. Natural restoration is suggested in this area. Vegetation growth in the karst areas is sensitive to water stress-related variables due to the particular geological and soil characteristics. The bidirectional causality relationship between vegetation greening and the environment factors in many of these areas indicates that the vegetation changes can also significantly affect water balance and conditions. Ecological engineering projects are suggested in this area. The vegetation growth in the SC Basin, HN, HB, GD, and eastern GX is also sensitive to water stress, while these regions are vulnerable to waterlogging. This study helps to improve our understanding of ecosystem management and promote sustainable development in southwestern China.

Keywords: vegetation greening; karst regions; remote sensing



Citation: Huang, K.; Wang, R.; Wu, W.; Wu, P.; Li, H.; Zeng, L.; Shao, J.; Liu, H.; Xu, T. Trend of Vegetation and Environmental Factors and Their Feedback in the Karst Regions of Southwestern China. *Sustainability* **2022**, *14*, 15941. <https://doi.org/10.3390/su142315941>

Academic Editors: Rajendra Prasad Shrestha and Pawan K Joshi

Received: 27 September 2022

Accepted: 25 November 2022

Published: 29 November 2022

Publisher's Note: MDPI stays neutral with regard to jurisdictional claims in published maps and institutional affiliations.



Copyright: © 2022 by the authors. Licensee MDPI, Basel, Switzerland. This article is an open access article distributed under the terms and conditions of the Creative Commons Attribution (CC BY) license (<https://creativecommons.org/licenses/by/4.0/>).

1. Introduction

Vegetation controls the exchange of carbon, water, and energy between the land and the atmosphere [1,2]. Vegetation variations result not only from climatic and environmental changes but also feed back to the climate through biogeochemical and biogeophysical processes [1,3]. Specifically, vegetation can hold topsoil in place with its root structures, and thus vegetation restoration can be a viable erosion control strategy [4,5]. Vegetation variations can also influence local and/or regional precipitation, run-off, and soil moisture by regulating evapotranspiration (ET) and the hydrologic cycle, which results in modification of the surface biogeophysical properties of the areas where the vegetation is growing at a local, regional, and even global scale [6–10]. Many studies have reported a greening vegetation trend both locally and globally, and particularly in China and India, as a result

of reforestation and agricultural intensification [1,3,11]. In addition, vegetation degradation or restoration can also reflect the condition of the ecological environment or the impact of human activity [12,13]. Therefore, the quantification of vegetation change and its biogeophysical feedback to the climate and ecosystem has elicited considerable interest from scientists and policymakers [1].

Karst is an area of land comprised of limestone [14]. In karst regions, the shallowness and discontinuity of the soil layers result in ecohydrological processes and water environments that are significantly distinct from most nonkarst regions [14–16]. Because of their poor stability and great fragility, karst ecosystems are susceptible to disturbance, which increases their sensitivity to environmental changes and human impacts [14,17]. Their vulnerability is characterized by the following three aspects: (1) Soil vulnerability, because of the scarcity of parent material, the soil formation process in karst areas is relatively slow [18]. (2) Hydrological vulnerability, the spatial separation of water and soil causes the fragility of hydrological systems in karst areas. (3) Vegetation vulnerability due to poor water and nutrient supply and the limited storage capacity of the soil layer.

In southwestern China, the karst area is located in tropical, subtropical, and temperate zones, covering an area of approximately 620,000 km² across several provinces [19–21]. It is one of the largest continuous karsts in the world and is also an area with the greatest concentrations of environmental impoverishment in China [16,17]. Because it is subjected to particular natural conditions as well as human impacts such as urbanization [21], overcultivation [22], etc., the Southwest China karst ecosystem is one of the most fragile areas [12,15,16,22,23]. Since the late 1990s, a series of ecological restoration projects, e.g., the Grain to Green Program and the Natural Forest Protection Project, have been implemented to restore vegetation cover in this area [22,24].

Satellite remote sensing observations collect image data globally and offer considerable potential for the characterization of spatiotemporal patterns and variations of vegetation, terrestrial water, evapotranspiration, precipitation, and soil moisture on a gridded basis. This can be achieved on a regional as well as a global basis in a consistent, efficient, and cost-effective manner [3,11,24]. Terrestrial water storage (TWS) data retrieved from the Gravity Recovery and Climate Experiment (GRACE) satellites were shown to be valuable for the investigation of groundwater depletion, interactions between vegetation and the hydrological environment [25–29], and for monitoring drought, fire, and flood disasters [30–32]. The data reflect all types of water stored across the continents, including surface water, soil water, groundwater, and canopy water [3]. Using time-series data derived from satellite imagery, many studies investigated spatiotemporal vegetation trends, the relationships between climatic change, vegetation change, ecological processes, etc. [33,34], and evaluated the effects of ecological restoration projects on vegetation conditions in southwestern China [22]. Because of its unique topographic conditions and ecological environment, even the temperature and precipitation patterns are spatially inconsistent, producing spatial and temporal variations in the vegetation conditions, biomass, and productivity within the region [35]. Therefore, vegetation variations and their interactions with environmental factors in the karst region of southwestern China are even more complex than in other regions and are worthy of in-depth study. These variations are critical to understanding the potential of ecosystem management interventions, such as reforestation and climate change mitigation [36,37].

Climate change and human activity are reported as the main forces driving vegetation change in this region [15,18,24,33,38–40]. Many studies reported that ecological protection projects significantly contributed to vegetation greening in the karst region of southwestern China [18,39,41]. Human activities such as deforestation, urbanization, and intensive agriculture also led to the degradation of the natural vegetation in this region [13,14,42]. Several studies reported that climate warming stimulated vegetation growth by enhancing its photosynthesis and extending the growing season, particularly in certain emerge-limited areas, e.g., high elevation plateaus [43]. Climate change was also identified as a negative factor restricting vegetation growth and even weakening the positive effect of human

activities in southern China [17,39,44]. In addition, previous studies showed that the karst landform and topography significantly influenced the combined effects of those driving factors and created a specific heterogeneous pattern of vegetation trends and changes in this region [18,35,42]. Vegetation changes also exerted an influence on climate and the ecosystem [1]. As a result, the interactions between vegetation and driving factors have become more complex and difficult to understand.

However, few studies have explored the TWS variations and their spatial–temporal relationships with the greenness of vegetation in Southwest China. Furthermore, previous studies have mainly focused on the one-way influences of climate change and human activity on vegetation changes, whereas the interaction between vegetation and environmental factors in the karst areas in southwestern China has been poorly understood. In particular, it remained unclear to what extent changes in the productivity of vegetation influenced the climate and environment, and this required further study. In addition, most studies focused on parts of the karst region of southwestern China [5,14,21,34] without large-scale application [43]. This paper aims to fill the research gap, by investigating: (1) trends in vegetation and climate change from 2001 to 2021 in the karst region of Southwest China; (2) the response (including the time-lag effect) of the vegetation to variations of the climate and environmental variables, such as terrestrial water, precipitation, and soil moisture; and (3) how vegetation changes have influenced ecosystem and environmental variations in this region. The results of this study provide scientific support for the restoration of vegetation in fragile ecological environments.

2. Materials and Methods

2.1. Study Area

The study area is located in Southwest China, covering the entire karst region of southwestern China and including eight provinces, i.e., Yunnan (YN), Chongqing (CQ), Sichuan (SC), Guangxi (GX), Hubei (HB), Guizhou (GZ), Hunan (HN), and Guangdong (GD) (Figure 1). This area has a tropical and subtropical monsoon climate, and the elevation generally increases from east to west. The highest point bordering the southeastern part of the Qinghai-Tibet Plateau is close to 6700 m above sea level, and the other areas are generally less than 3000 m above sea level.

Annual air temperature increases from northwest to southeast, whereas precipitation decreases from northwest to southeast, but both are extremely variable depending on geographical conditions [42,45]. Karst represents 28% of the study area, and this is underlain by exposed carbonate rocks [18]. According to the geological zoning, the study area can be divided into three parts: the non-karst area, the Qinghai-Tibet Plateau Zone karst area (hereafter QT Karst), and the Yunnan-Guizhou Plateau and southeast China hilly zone karst (hereafter YG Karst) (Figure 1). Karst landscapes are dominant in the Yunnan-Guizhou Plateau and the Guangxi Hills. There are various types of landforms in the region, such as plateaus, basins, hills, and plains. Eighty percent of the Sichuan Basin (SC Basin) is less than 2000 m above sea level, and 50% of the basin has been cultivated [42]. Rocky desertification mainly occurs in Yunnan, Guizhou, and Guangxi provinces and, in 2005, extended across 24% of the exposed carbonate rock area in this region [18]. Faced with the challenge of climate change and intensive anthropogenic disturbances, these fragile karst regions undergo severe soil erosion and rocky desertification [16,24].

2.2. Data Preparation and Processing

In order to explore the interactions between vegetation greening and environmental factors at the regional scale, several data products derived from satellite imagery were used in this study. These included some of the Moderate Resolution Imaging Spectroradiometer (MODIS) standard data products, such as the global evapotranspiration (ET) product (MOD16), the leaf area index product (MOD15A2H), and the LST and Emissivity product (MOD11A2). These datasets were accessed from the Google Earth Engine platform (GEE: <https://earthengine.google.com/platform/> (accessed on 28 June 2022)).

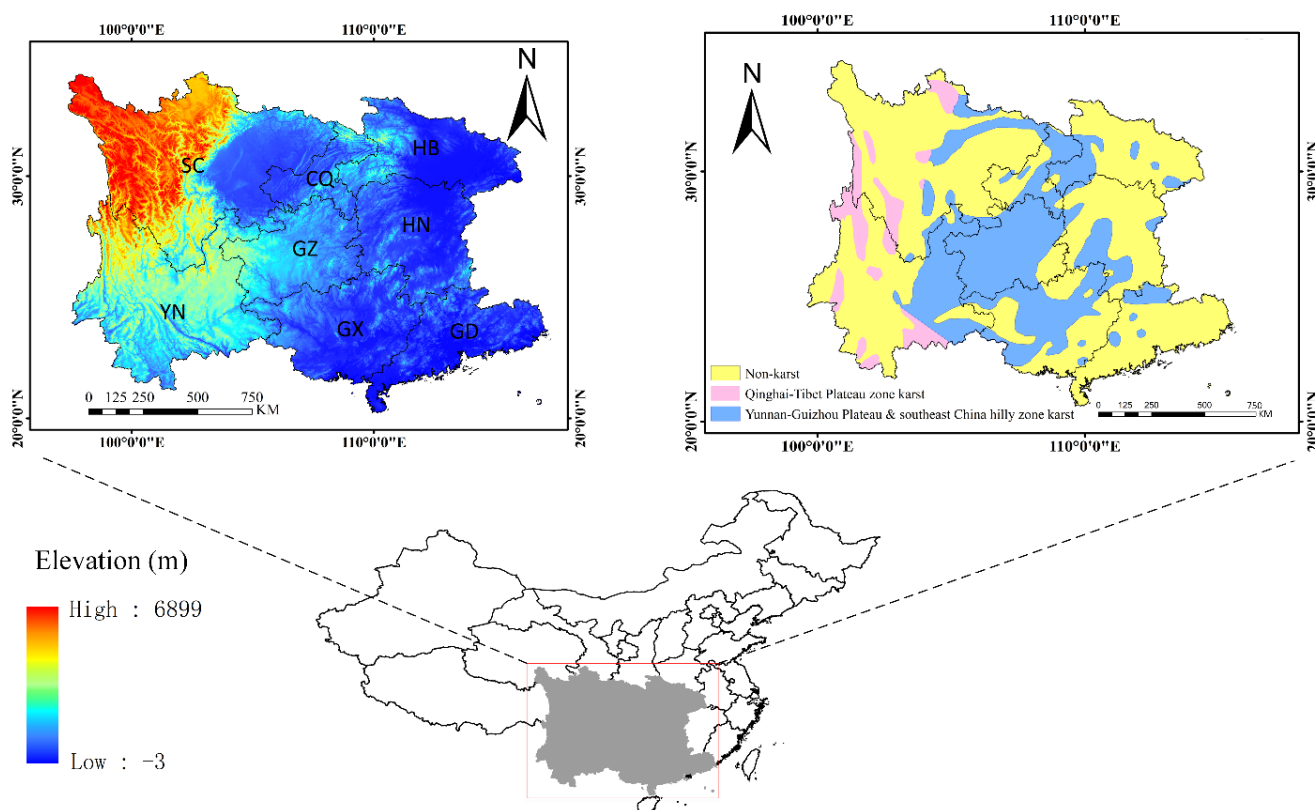


Figure 1. The geographical location, elevation, and karst environment in the study area.

2.2.1. Global Terrestrial Water Storage (TWS) Data

Monthly TWS data from 2003 to 2017 were used in this study. They were derived from the GRACE JPL mascons dataset produced by the Jet Propulsion Laboratory (JPL) based on the mascon method [46–48]. This product provides monthly gravity anomalies relative to a time-mean baseline (e.g., 2004–2009) and represents integrated changes in the land–water mass [49,50]. The dataset uses equivalent water thickness (EWT) to represent the vertical water mass anomalies in the centimeter unit (cm). It has a spatial resolution of $0.5^\circ \times 0.5^\circ$ nominally.

2.2.2. Evapotranspiration Data

In this study, we used the MOD16A2.006 ET product covering 2001 to 2021 with a temporal resolution of eight days and a spatial resolution of 500 m. The ET algorithm is based on the Penman–Monteith equation [51]. It provides ET, potential evapotranspiration (PET), and potential latent heat flux data. The ratio of ET to PET (ET/PET) was calculated to represent regional water and energy balances and soil water status.

2.2.3. Leaf Area Index (LAI) Data

The MOD15A2H product from 2001 to 2021 with a spatial resolution of 500 m and a temporal resolution of 8 days was used in this study to represent vegetation coverage and greening. It has been widely considered an important indicator for quantifying vegetation change trends [13,39].

2.2.4. Land Surface Temperature (LST) Data

The MOD11A2 product provides an 8-day composite daytime and nighttime LST with a spatial resolution of 1000 m. Daytime LST data covering 2001 to 2021 were used in this study. This product uses a split-window algorithm to retrieve daytime and nighttime LSTs [52].

2.2.5. Precipitation Data

The Tropical Rainfall Measuring Mission (TRMM) provides critical precipitation measurements (NASA: <https://gpm.nasa.gov/> (accessed on 28 June 2022)). The monthly precipitation product (TRMM 3B43) with 0.25° resolution from 2001 to 2019 was used in this study.

2.2.6. Soil Moisture (SM) Data

SM is a key parameter for understanding land surface hydrological processes. The “Daily all weather surface soil moisture data set with 1 km resolution in China” dataset covering 2003 to 2019 was used in this study [53]. It was generated by downscaling the SSM of AMSR-E and AMSR-2 to 36 km, with the primary inputs including MODIS reflectance data and daily LST data. Its coverage in China is almost complete from April to September, with significantly improved coverage in other months. The product was shown to be reliable when compared with against in situ soil moisture measurements from 2000+ meteorological stations in China.

2.2.7. Land Cover Classification Data

Global 30 m land cover dynamic monitoring products produced by the Aerospace Information Research Institute, Chinese Academy of Sciences (GLC_FCS30_1985-2020) were used in this study [54–56]. The data are generated by combining the full time series Landsat data from 1984 to 2020. The products contain 29 land cover classes with an update period of 5 years.

2.2.8. Data Processing

In order to standardize the resolution of the different datasets, the nearest neighbor method was employed to resample the datasets to a 1000 m resolution, with the exception of the TWS data. With regard to the GRACE TWS data, despite their $0.5^\circ \times 0.5^\circ$ nominal spatial resolution, their actual resolution of $3^\circ \times 3^\circ$ is much coarser than the other products. Hence, the datasets were all resampled to $0.5^\circ \times 0.5^\circ$ when analyzed with TWS data. All the MODIS products are available from January 2001 to December 2021, but some of the other products do not cover this entire period. In this study, the overlapping time periods of the two datasets were used when conducting combined analysis of two different datasets, such as the correlation and causality analysis.

2.3. Methodology

2.3.1. Calculation of Variable Anomalies

The strong seasonality of vegetation and environmental factors can significantly affect the study of their relationships. In order to remove the seasonality of these variables and as carried out in previous studies, the monthly anomalies were calculated by subtracting the corresponding multiyear mean values at pixel level [3,50].

2.3.2. Trend Analysis

The Mann-Kendall trend test [57] and univariate linear regression were used to perform trend analysis of the variables including LAI, TWS, ET, SM, LST, and precipitation. The Mann-Kendall trend test was applied first to detect trends. The trend is significant when the p -value is less than 0.05. If the trend is significant, the regression equation is obtained by linearly fitting the variables to time. The trends were evaluated by the slope of the regression equation.

2.3.3. Temporal Correlation Analysis

Pearson's correlation analysis was applied to examine the temporal correlation between vegetation greening and environmental factors. Given that there may be a time lag in the response of vegetation [25], a time lag of 0–6 months was applied in the correlation analysis by shifting the time series of environment variables to precede the LAI time series. The correlation was considered significant in this study when the p -value was less than 0.05. The maximum correlation between LAI and environmental factors was calculated by selecting the most significant correlation (maximum absolute value of the correlation coefficient) among the time series with a time lag of 0–6 months.

2.3.4. Granger Causality Analysis

Granger causality analysis [58] was used to analyze the interaction between vegetation greening and environmental variables [3,59]. The causal relationship between the variables x and y is expected to be tested twice in two directions. In order to test whether x is the cause of y , this method measures if prediction of a certain time-series (x) is significantly improved by including the past information of another time-series (y) by comparing Equations (1) and (2) [60]. That is, a F -test (Equation (3)) was used to examine whether there is a significant statistical difference between the estimates of Equations (1) and (2). If $F > F_\alpha$, then the null hypothesis does not stand, indicating that it is significantly different from zero, x is the Granger cause of y , and vice versa [3]. F_α is set to 0.05.

$$y_t = \sum_{i=1}^P \beta_i y_{t-i} + \sum_{i=1}^Q \alpha_i x_{t-i} + \varepsilon_i, \quad (1)$$

$$y_t = \sum_{i=1}^P \beta_i y_{t-i} + \varepsilon_i, \quad (2)$$

$$F = \frac{(RSS_r - RSS_u)/Q}{RSS_u/(N - P - Q - 1)} \propto F(Q, N - P - Q - 1), \quad (3)$$

where x and y are two time-series. P and Q denote the maximum lag periods for variables y and x , respectively. N is the sample size. α_i and β_i is the regression coefficients. ε_i is the error term. RSS_r and RSS_u represent the residual sum of the squares of Equations (1) and (2), respectively.

3. Results

3.1. Change Trends

3.1.1. Land Cover Changes

As shown in Figure 2, southwestern China is dominated by forests (~50%). Grassland is mainly distributed in the Hengduan Mountains and the Zoige Plateau in northwestern SC. The cropland in the study area is mainly distributed in the SC Basin at the junction of SC and CQ, the Jiangnan Plain in HB, and the Dongting Lake Plain at the junction of HB and HN, as well as in the Guangxi Basin in GX. During the two decades from 2000 to 2020, the distribution patterns of different land use types did not fundamentally change. Forest and cropland areas decreased slightly, with net losses of 1% and 2% of the total areas, respectively, whereas shrubland areas increased by 1% from 5% to 6%. Grassland areas distributed in northwest SC remained basically stable. However, the urban areas expanded significantly, with the proportion increasing from 1% to 3%. The land use in the QT Karst area shows obvious differences with non-karst or YG Karst areas (Figure 2c–e), though little difference is found between the land cover proportions in non-karst and YG Karst areas. QT Karst area has extensive grassland (32%) than non-karst (14%) or YG-karst area (9%), whereas cropland accounts for much greater percentage in non-karst (27%) or YG-karst area (25%) than in QT Karst area (4%) where is sparsely populated.

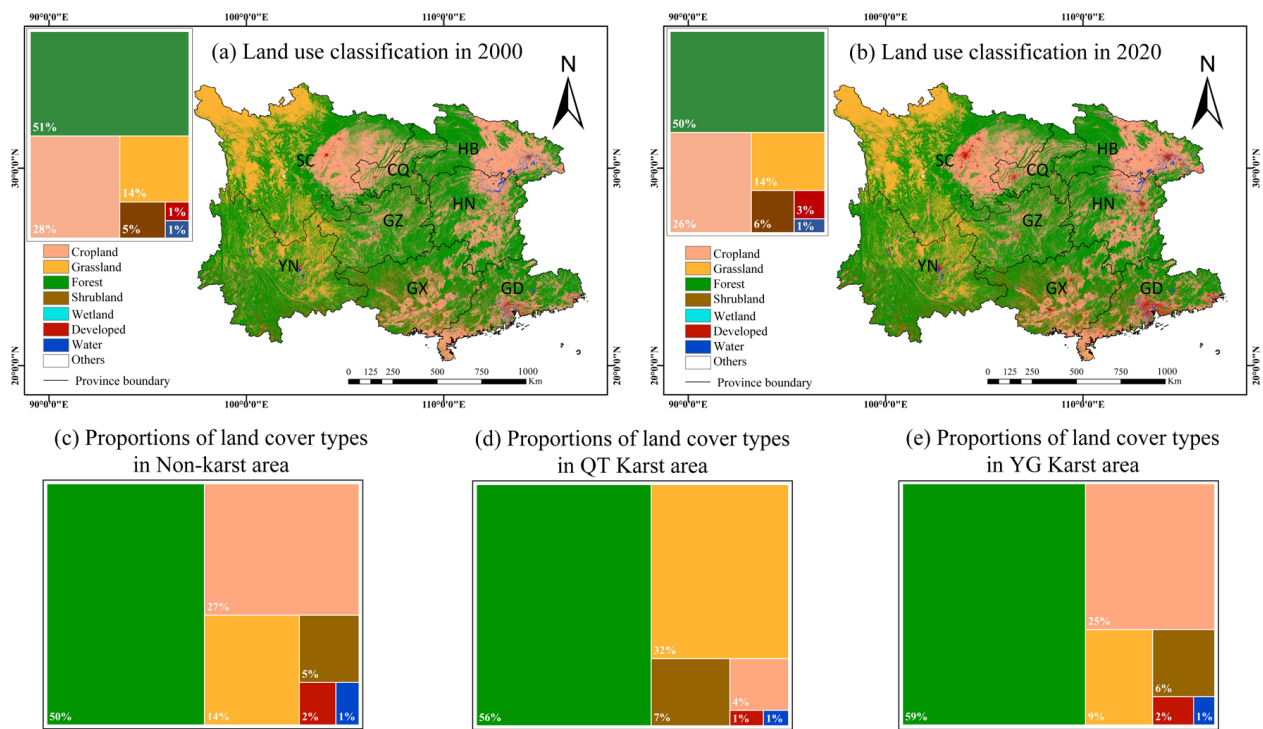


Figure 2. Spatial patterns and statistics of land use classification in southwestern China in (a) 2000 and (b) 2020, and the statistics of land cover types in (c) Non-karst, (d) QT Karst, and (e) YG Karst areas.

Figure 3 shows the proportions of cropland, grassland, and forest that changed to other types of land cover during the four time periods from 2001 to 2020. First, cropland areas have continuously decreased. Annually, ~2.4% of the loss of cropland area during the period from 2001 to 2020 resulted from conversion to urban land use because of rapid urbanization during this period. The increase in forest, grassland, and shrubland accounted for ~50% of the total loss of cropland area during the period from 2001 to 2020. During this period, many afforestation and conservation projects were implemented that converted some farmland and degraded land back to substantial natural land resources, such as forests, grassland, and shrubland [17,39,61]. Second, most of the loss of grassland area (~70%) resulted from conversion to forest, in particular from 2001 to 2005, because of afforestation projects conducted during this period. Some of the area was converted to urban land and cropland. Third, the forest area decreased, mainly as a result of conversion to cropland, shrubland, and grassland, which accounted for 34%, 41%, and 18%, respectively. The forest degradation and conversion to other land cover types were reported as the combined effects of climate change and human activities [17], such as the conversion of forest land for agriculture [42,62,63].

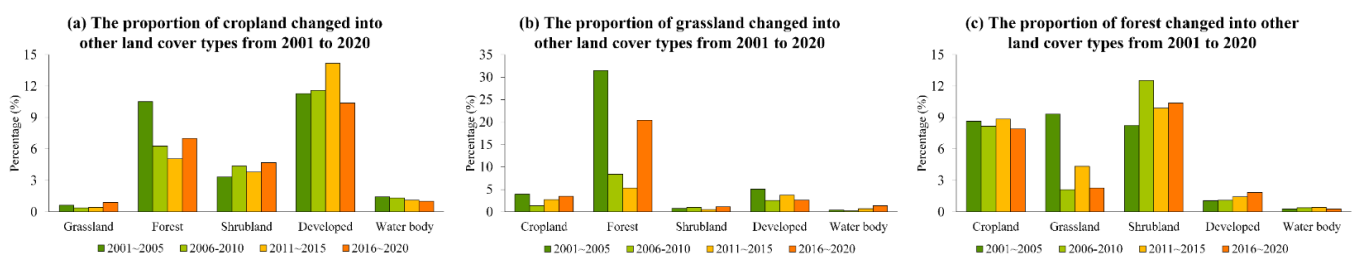


Figure 3. The proportion of (a) cropland, (b) grassland, and (c) forest changed into other land cover types in Southwest China from 2001 to 2005 (dark green bar), from 2006 to 2010 (light green bar), from 2011 to 2015 (yellow bar), and from 2016 to 2020 (orange bar).

3.1.2. Trend of Vegetation Greenness

Most regions of the study area showed a greening trend, and the greening of cropland, forests, and shrubland was most significant during the period from 2001 to 2021 (Figure 4). About 75%, 66%, and 72% of the cropland, forests, and shrub land areas showed a greening trend, respectively (Figure 5). YG Karst areas show greater greening proportions than non-karst or QT Karst areas. However, from 2001 to 2011, there were still some areas showing a decreasing trend in LAI (Figure 4). These areas were consistent with the areas and patterns of rocky desertification observed in previous studies [18], which were mainly driven by human activities and climate change. Far fewer areas demonstrated a significant trend of vegetation browning during the period from 2012 to 2021 (Figures 4 and 5). However, during the past ten years, the average vegetation greenness of some cropland in the Dongting Lake Plain at the junction of HN and HB has decreased (Figure 4).

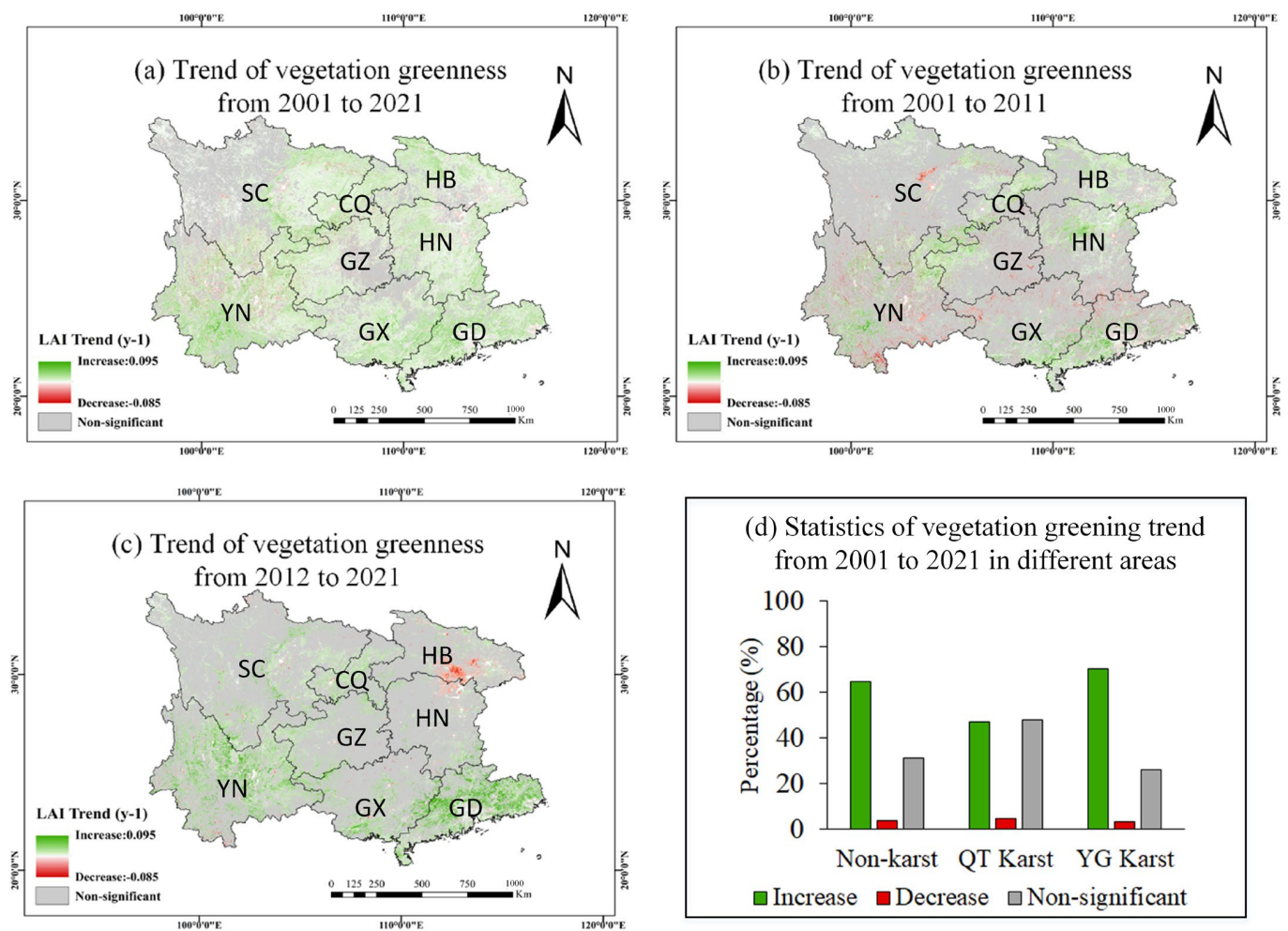


Figure 4. Spatial patterns of vegetation greenness trends in terms of LAI in Southwest China from (a) 2001 to 2021, (b) 2001 to 2011, (c) 2012 to 2021, and (d) the statistics of vegetation greening trend from 2001 to 2021 in Non-karst, QT Karst, and YG Karst areas.

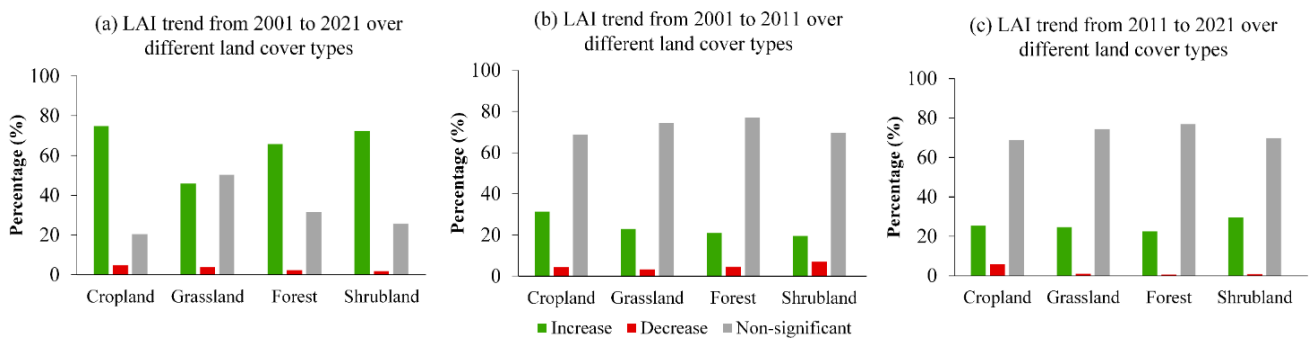


Figure 5. Statistics of vegetation greenness trend in terms of LAI in Southwest China (a) from 2001 to 2021, (b) from 2001 to 2011, and (c) from 2012 to 2021.

3.1.3. Trend of Vegetation Greenness Drivers

Trend of TWS

TWS is considered to be a hydrological factor that has a greater impact on vegetation growth than precipitation or soil moisture [3,25–29]. As shown in Figure 6, TWS in southwestern China (with the exception of the western high mountains) showed an increasing trend in the 15 years since 2003. The western high mountains showed a decreasing trend of TWS, in particular during the period from 2003 to 2011. As shown in Figure 6d, about 96% of the YG Karst area showed an increasing trend in TWS, while about 62% of the QT Karst area showed a decreasing trend. This may be related to snowmelt on the high mountains. During the period from 2012 to 2017, TWS in most of the regions showed a more rapid increasing trend than in the previous decade, especially in YN, GZ, and HN.

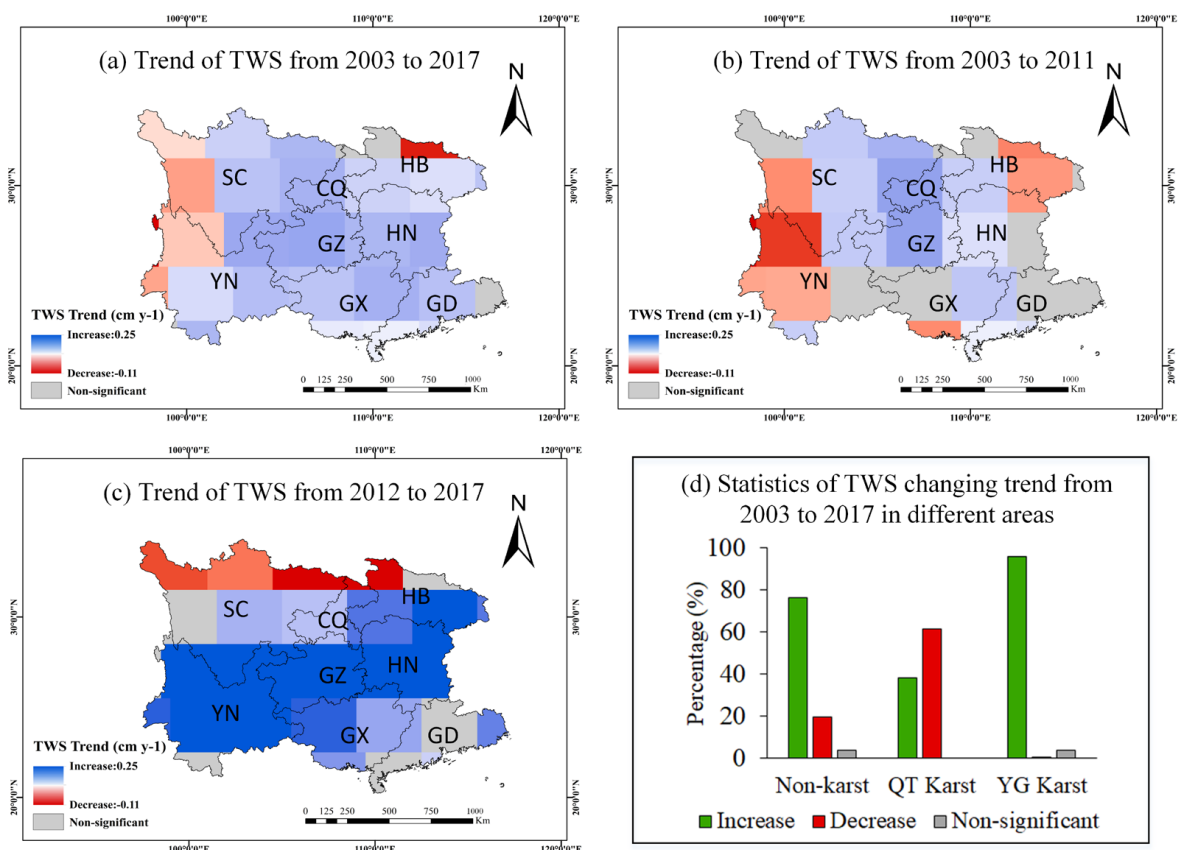


Figure 6. Spatial patterns of TWS trend in Southwest China from (a) 2003 to 2017, (b) 2003 to 2011, (c) 2012 to 2017, and (d) the statistics of TWS changing trend from 2003 to 2017 in Non-karst, QT Karst, and YG Karst areas.

Trend of SM

The soil moisture trend in Southwest China from 2003 to 2019 is shown in Figure 7. During this period, a slight decreasing trend in SM was observed in the northeast of the study area, including the SC Basin, HB, HN, and eastern GZ, whereas a slightly increasing trend was found in the south of the study area. Compared to the non-karst and YG Karst areas, obvious lower proportion of the QT Karst area showed a decreasing trend in SM. The spatial pattern of the SM trend during the period from 2001 to 2011 was different from that for the period from 2012 to 2019. The more recent decade showed a more rapidly decreasing SM trend in the east of the study area compared with the previous decade, especially in GX and GD, where opposite trends were observed in two decades. However, in the west of the study area, in western SC and some regions of YN, a significant increasing trend was observed in the last decade.

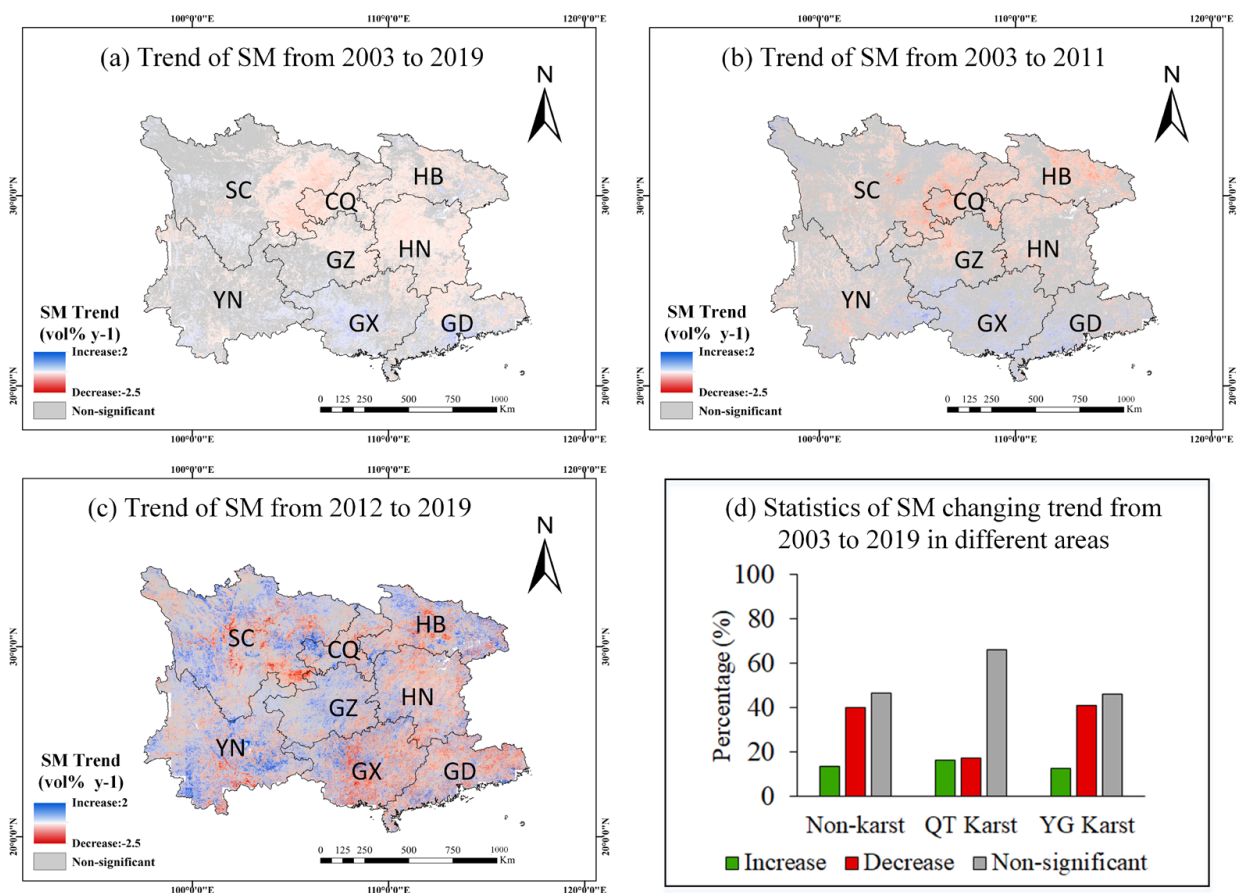


Figure 7. Spatial patterns of SM in Southwest China from (a) 2003 to 2019, (b) 2003 to 2011, (c) 2012 to 2019, and (d) the statistics of SM changing trend from 2003 to 2019 in Non-karst, QT Karst, and YG Karst areas.

Trend of Precipitation

As shown in Figure 8, most of the regions in Southwest China showed nonsignificant trends in terms of precipitation changes from 2001 to 2019. The alpine area of northwestern YN showed a decreasing trend of precipitation. An increasing trend of precipitation was observed in several regions, such as northwestern SC, the area bordering YN and GZ, and the area bordering GZ and GX. Although precipitation in some local areas, such as central and southeastern YN and southern HN, showed a downward trend from 2001 to 2011, few areas with significant precipitation change trends were found in the study area during the period from 2012 to 2019.

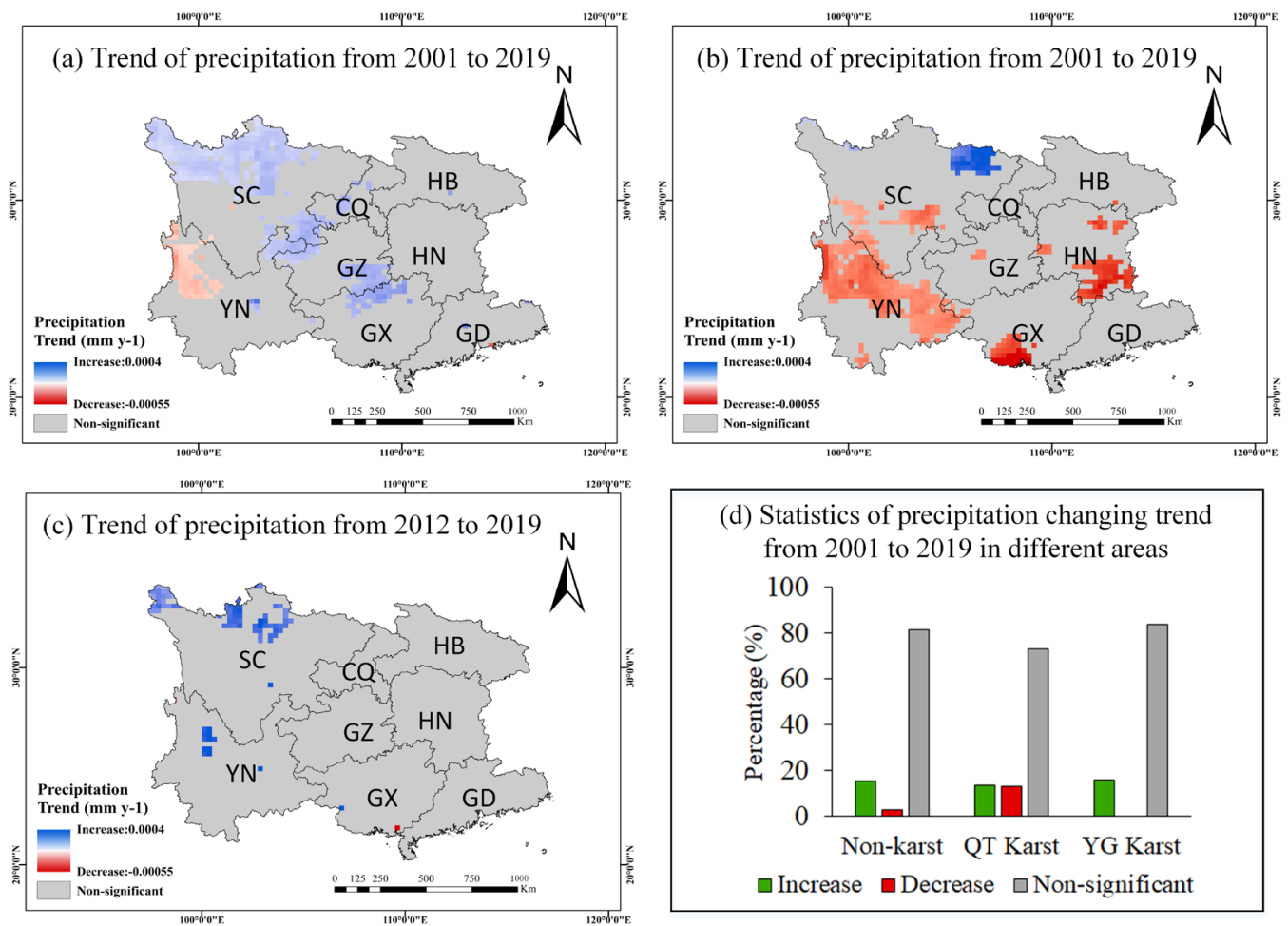


Figure 8. Spatial patterns of precipitation in Southwest China from (a) 2001 to 2019, (b) 2001 to 2011, (c) 2012 to 2019, and (d) the statistics of precipitation changing trend from 2003 to 2019 in Non-karst, QT Karst, and YG Karst areas.

Trend of the ET/PET Ratio

As shown in Figure 9, the ET/PET ratio, i.e., water conditions, in most areas showed a slightly increasing trend. The increasing trend was more rapid in the cropland of the SC and Guangxi Basins. During the period from 2001 to 2011, the ET/PET ratio showed an increasing trend in some of the central regions and a decreasing trend in the high mountains of western SC. However, there were no significant changes in trends in most of the other regions during this period. From 2012 to 2021, most of the western region, in particular the SC Basin and the western Hengduan Mountains, showed a more significant increasing trend. However, the ET/PET ratio showed a significant downward trend in GD during the period from 2012 to 2021 (Figure 9), although this region showed an obvious greening trend during the same period (Figure 4).

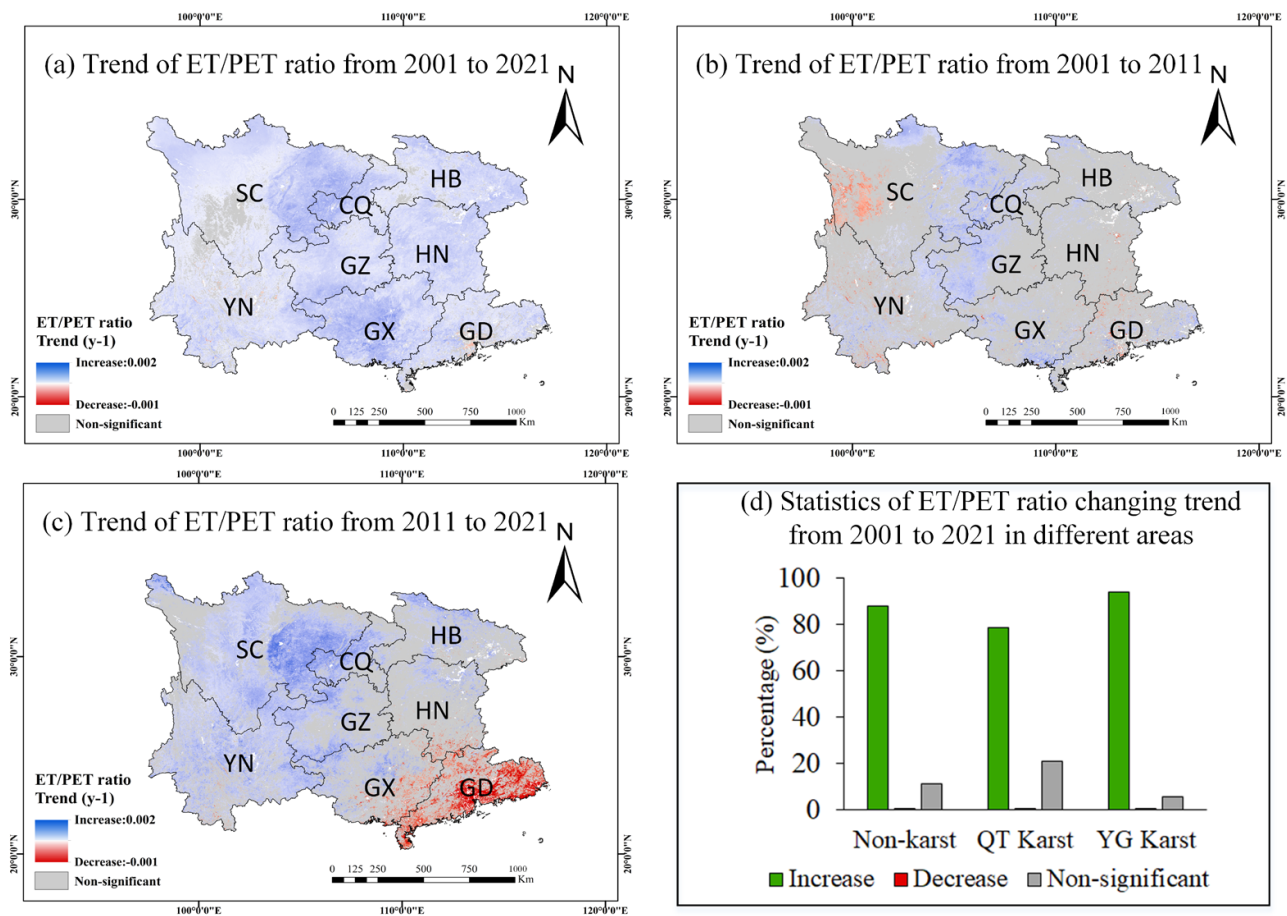


Figure 9. Spatial patterns of ET/PET ratio in Southwest China from (a) 2001 to 2021, (b) 2001 to 2011, (c) 2012 to 2021, and (d) the statistics of the ET/PET ratio changing trend from 2003 to 2019 in Non-karst, QT Karst, and YG Karst areas.

LST Trend

The trend of LST change in southwestern China from 2001 to 2021 is shown in Figure 10. LST in the SC Basin showed a continuously increasing trend during the period from 2001 to 2021. Compared to LST changes during the period from 2001 to 2011, LST from 2012 to 2021 revealed a more rapid warming trend in most regions of the study area apart from YN. In particular, the LST in the east of the study area, including some regions in HN, HB, GD, and GX, showed a significant increasing trend from 2012 to 2021, which led to an increasing trend throughout the period from 2001 to 2021, even though there was no obvious trend of change in most parts of these regions from 2001 to 2011. A significant increasing trend in the LST was observed from 2001 to 2021 in alpine areas, i.e., western SC and western YN. Specifically, the LST showed a significant increasing trend during the period from 2001 to 2011 in some of these areas but a significant decreasing trend in the following decade, both of which were consistent with the TWS trend in these regions. This points to the relationship between LST increase and TWS loss, as some of these areas are covered by snow, and snow melt occurs in the warmer parts of these areas because of the increase in LST [42,64]. The melted water from the snow-capped mountains flows into rivers such as the Jinsha, Lancang, and Nujiang Rivers, resulting in the loss of TWS in this region.

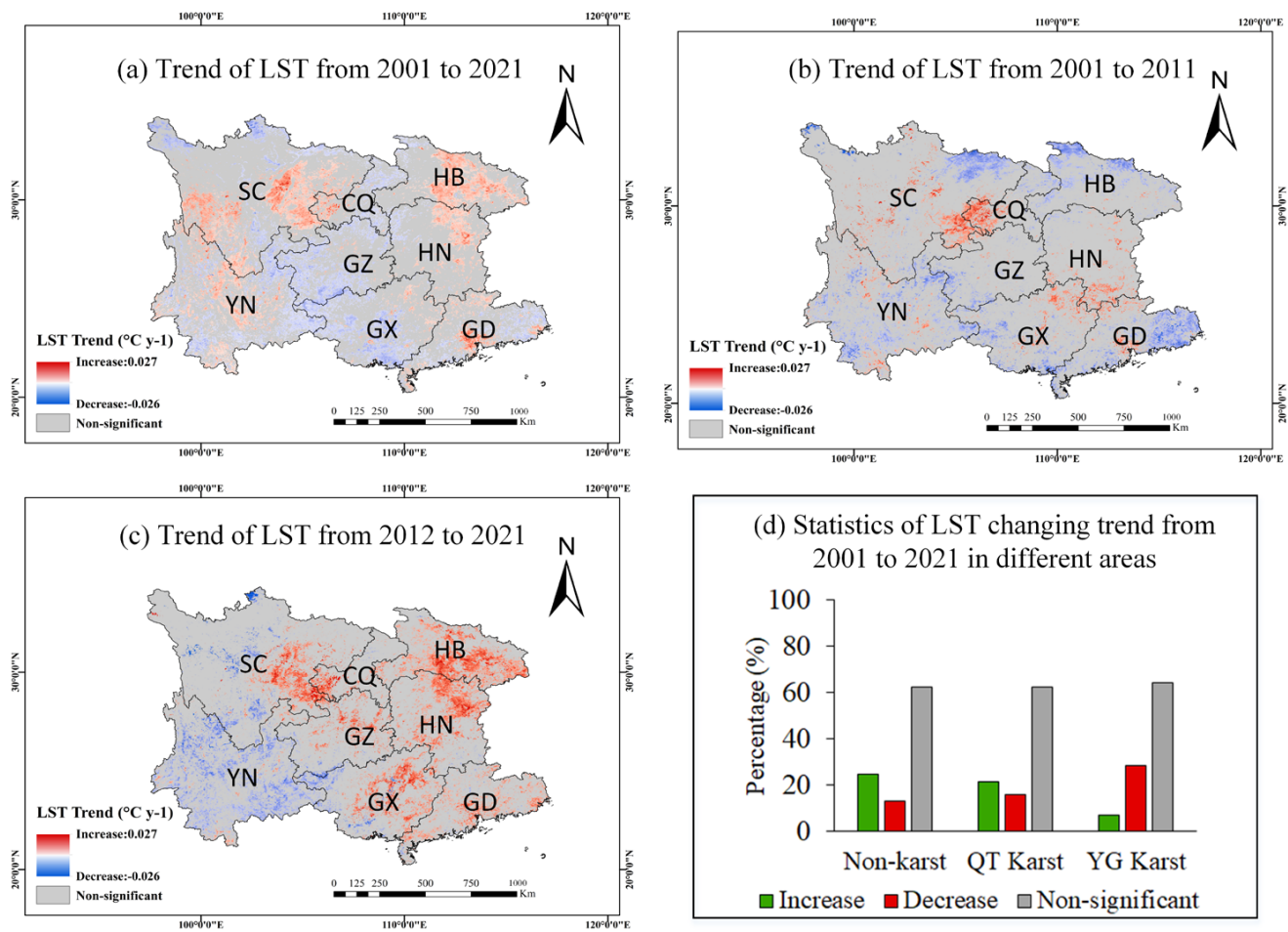


Figure 10. Spatial patterns of LST in Southwest China from (a) 2001 to 2021, (b) 2001 to 2011, (c) 2012 to 2021, and (d) the statistics of the LST changing trend from 2003 to 2019 in Non-karst, QT Karst, and YG Karst areas.

3.2. Correlation between Vegetation Greenness and the Driving Factors

3.2.1. Correlation between Vegetation Greenness and TWS

Figure 11 shows the maximum correlation efficiency values between LAI and TWS with a time lag of 0–6 months and the corresponding time lag with the maximum correlation efficiency between LAI and TWS. LAI was positively correlated with TWS in most regions in the non-karst and YG Karst areas. This indicates that water is still a key factor affecting vegetation growth in these regions. However, some alpine regions in the Hengduan Mountains at the junction of northwestern YN and southwestern SC showed a negative correlation between LAI and TWS. In addition to the Hengduan Mountains, two small local areas in northern HB and southeastern GD also showed a negative relationship between LAI and TWS. These regions where LAI was negatively correlated to TWS had an obviously shorter time lag than the regions where LAI had a positive correlation to TWS (Figure 11). However, LAI has a 2- to 3-month time lag in relation to TWS in the SC Basin, Guangxi Basin, other cropland-concentrated areas, and most forest regions in YN. The forest area surrounding the SC Basin has a clear 5- to 6-month time lag in relation to TWS.

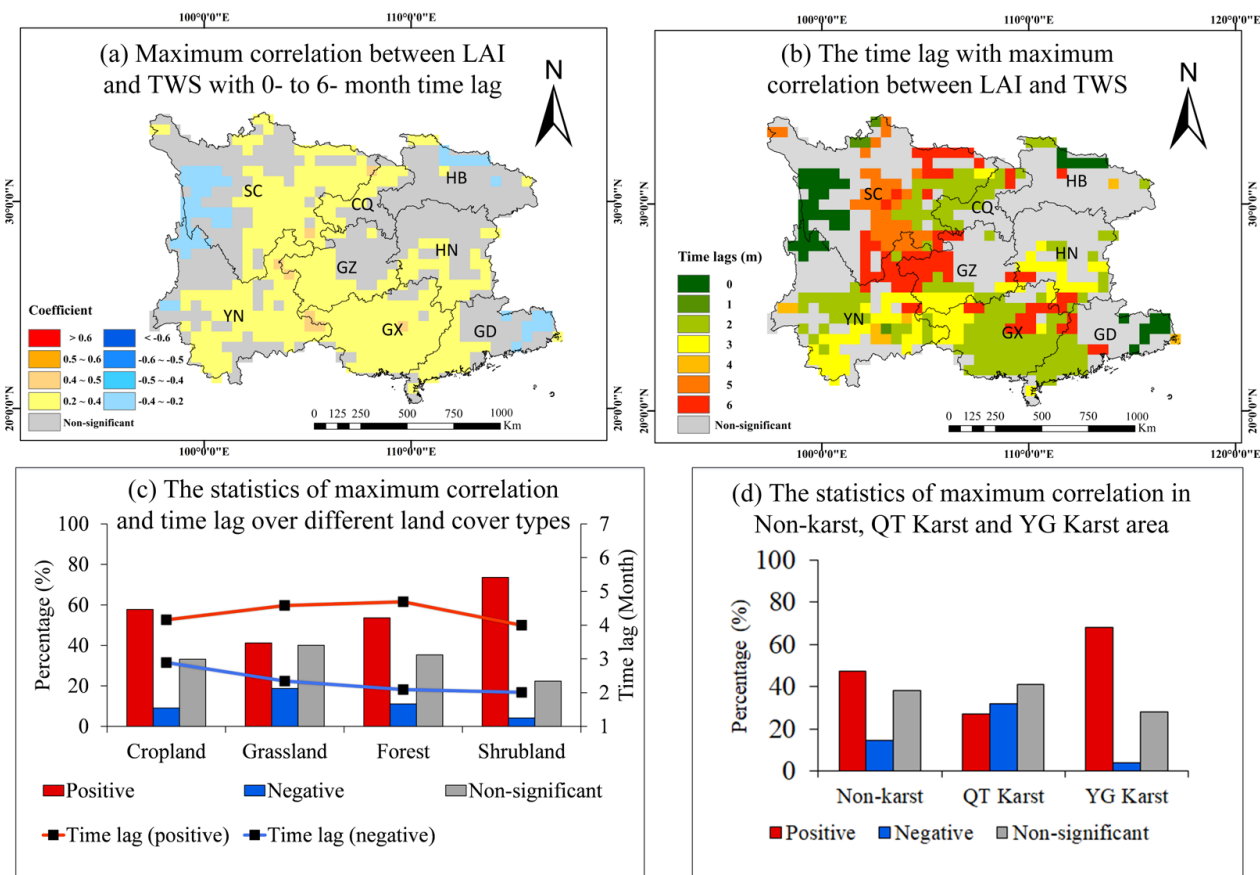


Figure 11. Spatial patterns of maximum correlation between LAI and TWS with (a) a 0- to 6-month time lag, (b) the corresponding time lag, and the statistics of maximum correlation and time lag for (c) different land cover types and (d) different karst areas in Southwest China.

As shown in Figure 11c, the responses of LAI to TWS also varied according to land cover type. The positive correlation of LAI to TWS was most observed in shrubland, followed by cropland, forest, and grassland, whereas the negative correlation of LAI to TWS was most observed in grassland, followed by forest, cropland, and shrubland. That is to say, shrubland tended to have more positive correlations to TWS than the other land cover types, whereas grassland tended to have more negative correlations to TWS than the other land cover types. This is because grasslands are mainly distributed in the western, energy-limited alpine areas, whereas shrublands are mainly located in the water-limited YG Karst regions.

3.2.2. Correlation between Vegetation Greenness and SM

Figure 12 shows the maximum correlation between LAI and SM with a time lag of 0 to 6 months and the corresponding time lag with the maximum correlation between LAI and SM. There was little difference between different geological zonings. There was no significant correlation between LAI and SM in GZ and western SC, but a positive maximum correlation was observed in some southern regions in YN, GX, and GD. A negative maximum correlation was found in HN and the SC Basin, whereas a significant positive maximum correlation between LAI and TWS was observed. LAI in HN had a rapid negative response to SM variations, which might be related to the influence of waterlogging and even flooding in HN. In the SC Basin, the responses of LAI had a 5- to 6-month time lag in relation to SM.

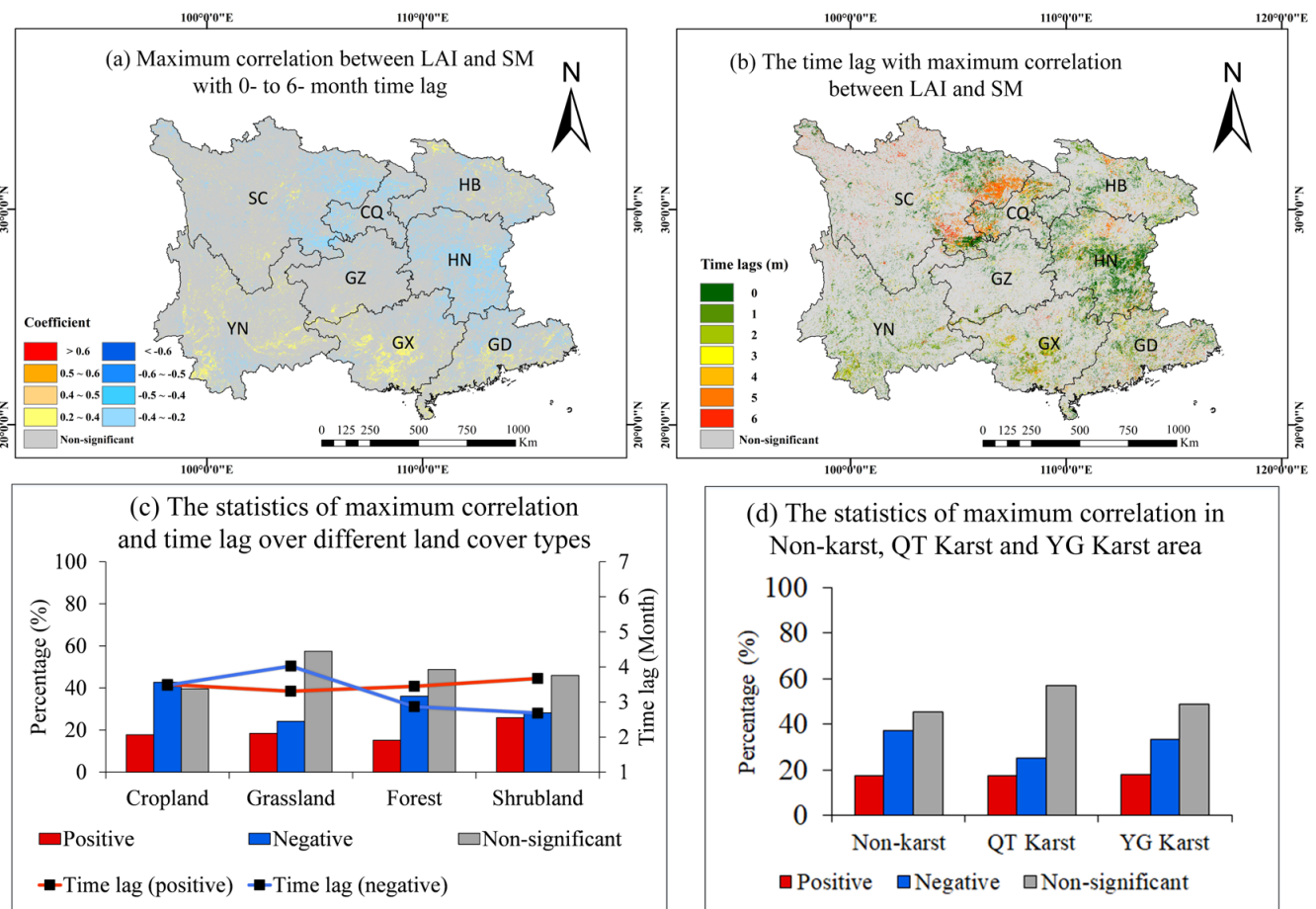


Figure 12. Spatial patterns of maximum correlation between LAI and SM with (a) a 0- to 6-month time lag, (b) the corresponding time lag, and the statistics of maximum correlation and time lag for (c) different land cover types and (d) different karst areas in Southwest China.

3.2.3. Correlation between Vegetation Greenness and Precipitation

Figure 13 shows the maximum correlation between LAI and precipitation with a 0- to 6-month time lag and the corresponding time lag with the maximum correlation between LAI and precipitation. Compared to non-karst and QT Karst areas, a greater proportion of the YG Karst area showed a positive correlation and a lower proportion showed a negative correlation between LAI and precipitation. The most significant relationship between LAI and precipitation was negative during the period from 2001 to 2019 in the southeast and western parts of the study area (such as GD, eastern GX, eastern HN, and western SC), and southern YN. In addition, LAI showed rapid responses to precipitation with a short time lag in these areas (≤ 1 month). In some local areas of the central karst regions and the SC Basin, LAI is positively correlated with precipitation. The cropland distributed in the SC Basin has a large water demand. Thus, the vegetation in these regions is sensitive to precipitation. In addition, the time lags of LAI to precipitation in these regions were obviously longer than in the areas where the most significant correlation between LAI and precipitation was negative (2.6 months compared to 1.2 months).

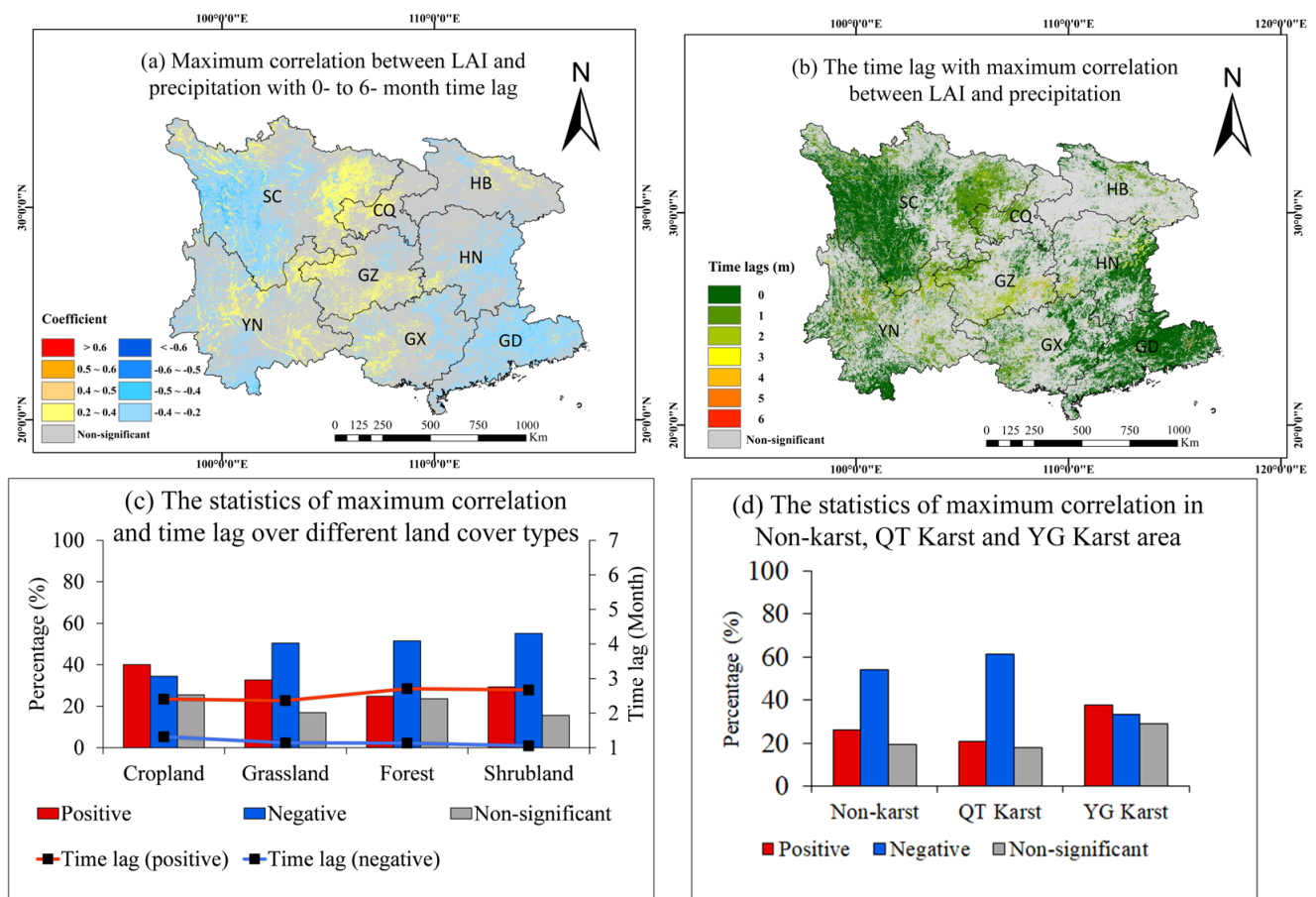


Figure 13. Spatial patterns of maximum correlation between LAI and precipitation with (a) a 0- to 6-month time lag, (b) the corresponding time lag, and the statistics of maximum correlation and time lag for (c) different land cover types and (d) different karst areas in Southwest China.

3.2.4. Correlation between Vegetation Greenness and the ET/PET Ratio

Figure 14 shows the maximum correlation between LAI and the ET/PET ratio with a 0- to 6-month time lag and the corresponding time lag with the maximum correlation between LAI and the ET/PET ratio. There was a significant positive correlation between LAI and the ET/PET ratio in most areas, with the exception of the western, energy-limited alpine areas of SC, where a significant negative correlation between LAI and the ET/PET ratio was observed. There was no obvious time lag in most areas where a significant correlation was found between LAI and the ET/PET ratio, i.e., LAI quickly responded to the changes in the ET/PET ratio.

3.2.5. Correlation between Vegetation Greenness and LST

Figure 15 shows the maximum correlation between LAI and LST with a 0- to 6-month time lag and the corresponding time lag with the maximum correlation between LAI and LST during the period from 2001 to 2021. The western Hengduan Mountains and the Zoige Plateau, with their high elevations and low temperatures, showed a positive correlation between LAI and LST, and the response of vegetation growth to changes in LST is rapid with a short time lag. However, in most of the other regions, no significant correlation between LAI and LST with a 0- to 6-month time lag was observed, with the exception of some areas in southern GX and GD where LAI was negatively correlated with LST. But the responses of LAI to the increase in temperature show an obvious time lag of 3 to 4 months. The possible reason for this might be a time lag in the vegetation's response to water stress caused by the rising temperature.

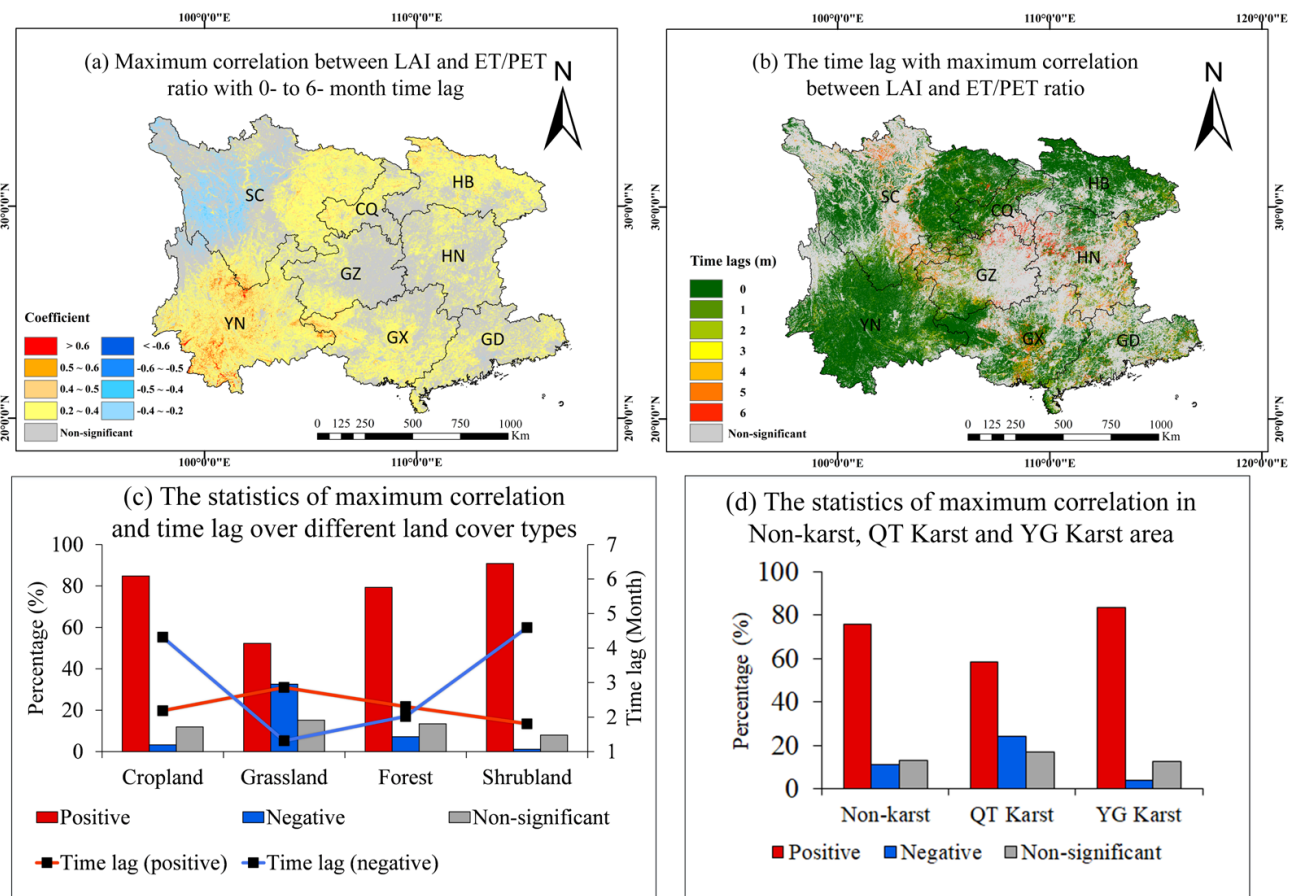


Figure 14. Spatial patterns of maximum correlation between LAI and the ET/PET ratio with (a) a 0- to 6-month time lag, (b) the corresponding time lag, and the statistics of maximum correlation and time lag for (c) different land cover types and (d) different karst areas in Southwest China.

3.3. Causal Link between Vegetation Greenness and the Driving Factors

3.3.1. Causal Link between Vegetation Greenness and TWS

The Granger causality relationship between the LAI and TWS is shown in Figure 16. Causality relationships between LAI and TWS were observed spatially in the YG karst regions (>50%). Bidirectional causality relationships were found in the YG Karst area in eastern YN and western GZ. TWS was found to be the unidirectional cause of LAI in the Guangxi Basin because the improvement of regional hydrological conditions has promoted vegetation greening there. LAI was found to be the unidirectional cause of TWS in the high-elevation forest area in south-central SC and the high-elevation grassland in northwestern SC. This indicates that vegetation changes can significantly affect water conditions in these high mountains. There was no significant causal relationship between LAI and TWS in most areas of HN and HB. In addition, clear differences were identified in the causal relationships between LAI and TWS with regard to different land cover types. The largest and most significant causality relationships were found for grassland (~60%) and least significant for forest (~40%). A possible reason might be that forest is less sensitive to water conditions than grassland.

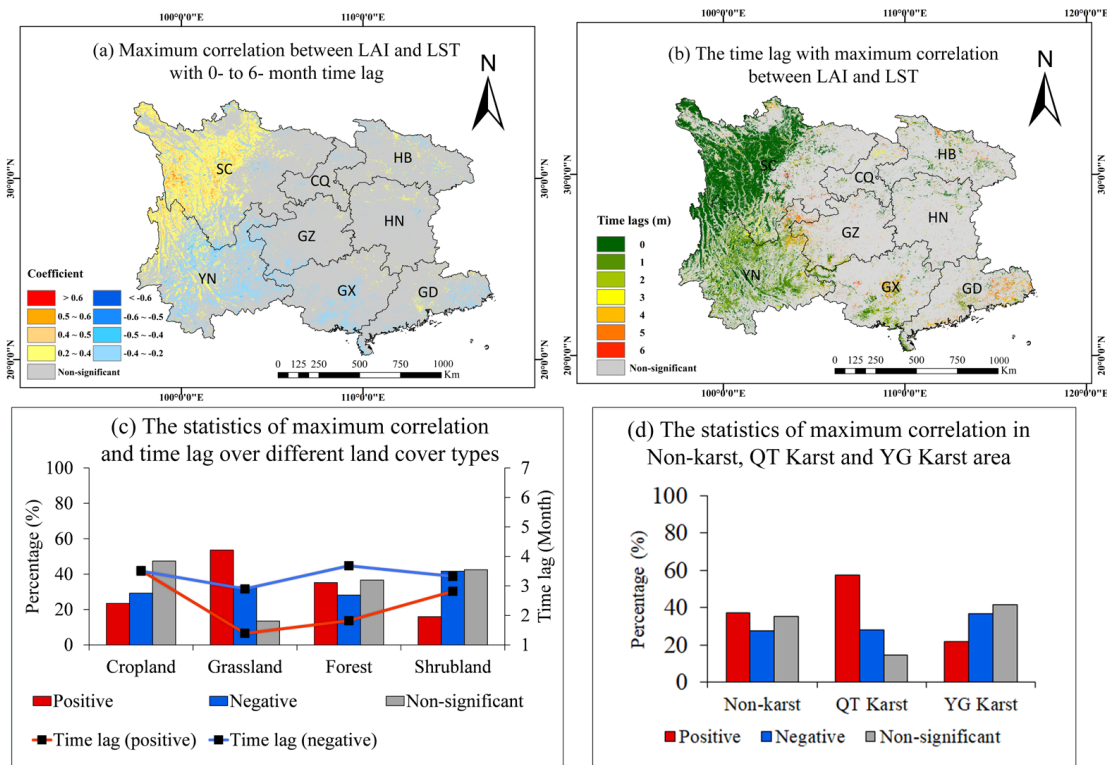


Figure 15. Spatial patterns of maximum correlation between LAI and LST with (a) a 0- to 6-month time lag, (b) the corresponding time lag, and the statistics of maximum correlation and time lag for (c) different land cover types and (d) different karst areas in Southwest China.

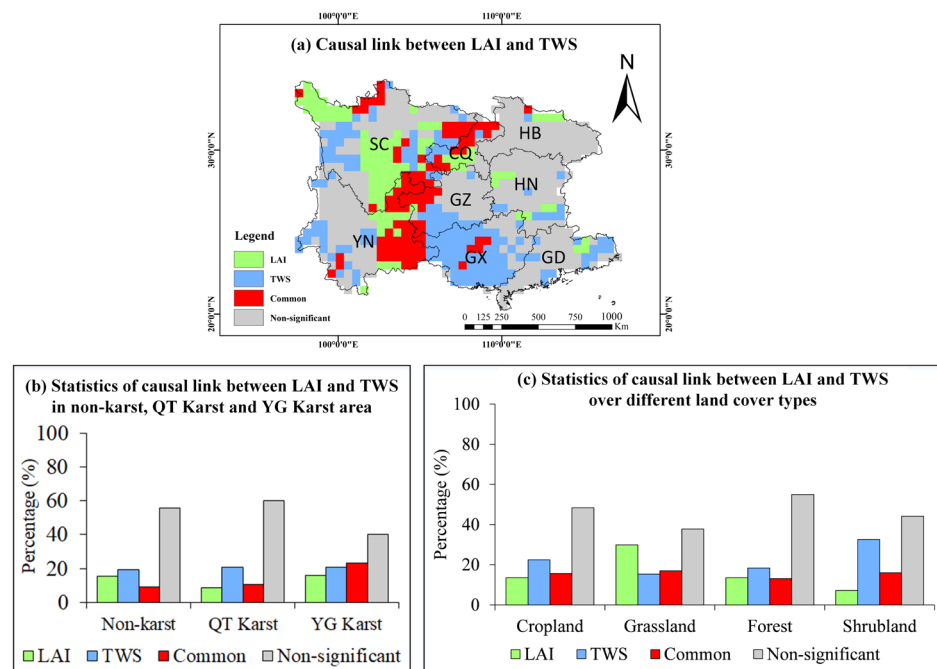


Figure 16. (a) Spatial patterns and statistics of the causality relationship between LAI and TWS over (b) different karst areas and (c) different land cover types in Southwest China. The red indicates bidirectional causal relationships between LAI and TWS; the blue indicates that TWS is the unidirectional cause of LAI; the green indicates that LAI is the unidirectional cause of TWS; the grey shows that there are no significant causal links between LAI and TWS.3.3. Interactions between vegetation greenness and SM.

3.3.2. Causal Link between Vegetation Greenness and SM

The Granger causality relationship between the LAI and SM is shown in Figure 17. Most of the regions (>60%) showed no significant causal relationship between LAI and SM with regard to the three geological zonings (Figure 17b) or four main land cover types (Figure 17c). LAI was the unidirectional cause of SM in most of the areas in southwestern China where there was a significant causal relationship between LAI and SM. This indicates that vegetation restoration in this area can influence the land-water conditions because vegetation is able to hold topsoil in place with its root structures, and vegetation restoration is therefore conducive to erosion control.

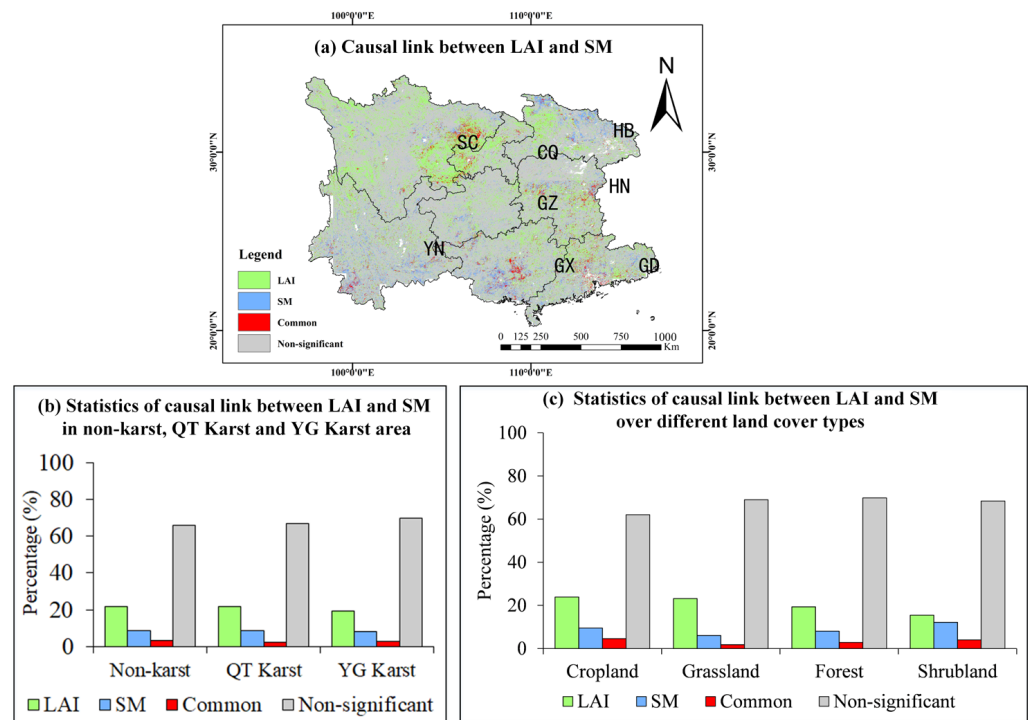


Figure 17. (a) Spatial patterns and statistics of the causality relationship between LAI and SM over (b) different karst areas and (c) different land cover types in Southwest China. The red indicates bidirectional causal relationships between LAI and SM; the blue indicates that SM is the unidirectional cause of LAI; the green indicates that LAI is the unidirectional cause of SM; the grey shows that there are no significant causal links between LAI and SM.

3.3.3. Causal Link between Vegetation Greenness and Precipitation

The Granger causality relationship between LAI and precipitation is shown in Figure 18. The spatial pattern of the causal link between vegetation greenness and precipitation is similar to that of the maximum correlation between them. Precipitation was found to be the unidirectional cause of the LAI in most areas in relation to the four main land cover types. There was little difference in the causal relationship between LAI and precipitation in the three geological zonings (Figure 18b) or over the three land cover types: cropland, grassland, and shrubland, though obviously a lower proportion of forest land showed that precipitation is the unidirectional cause of LAI changes than those of the other three land cover types. As the trees in forest land with deep roots are generally not as sensitive to water stress as other plants.

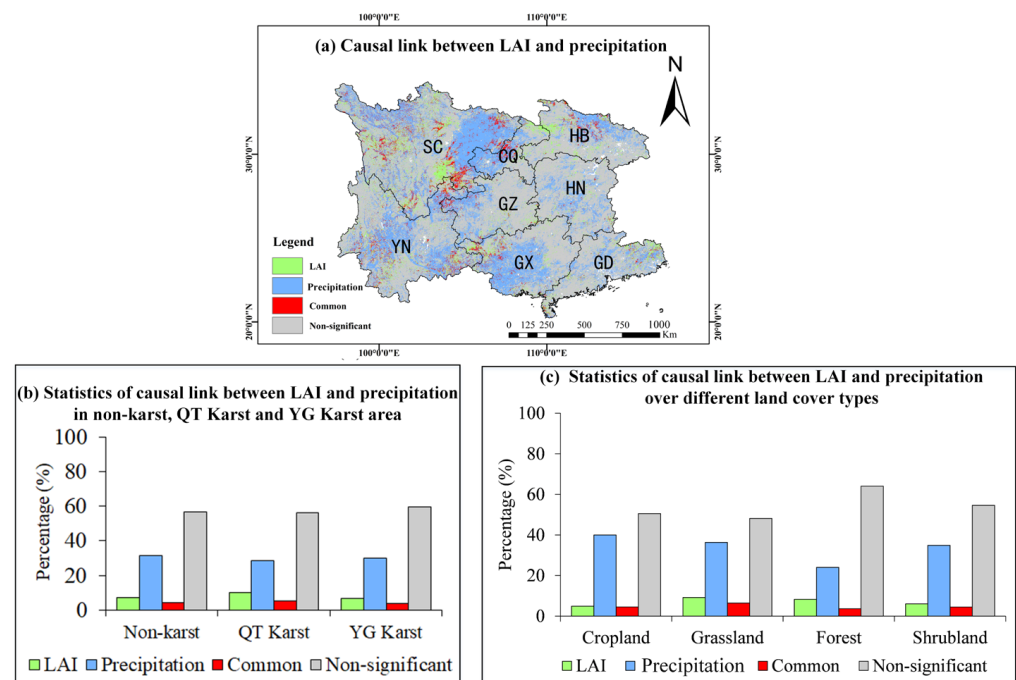


Figure 18. (a) Spatial patterns and statistics of the causality relationship between LAI and precipitation over (b) different karst areas and (c) different land cover types in Southwest China. The red indicates bidirectional causal relationships between LAI and precipitation; the blue indicates that precipitation is the unidirectional cause of LAI; and the green indicates that LAI is the unidirectional cause of precipitation; the grey shows that there are no significant causal links between LAI and precipitation.

3.3.4. Causal Link between Vegetation Greenness and the ET/PET Ratio

The Granger causality relationship between the LAI and the ET/PET ratio is shown in Figure 19. Most of the northwestern alpine regions are grassland, and there was no significant causal relationship between LAI and ET/PET with the exception of some valleys with low elevations, where variations in the ET/PET ratio were the cause of LAI changes. In most of the other areas of the study area, such as HN, northern HB, the SC Basin, the central and eastern Yunnan-Guizhou Plateau, and the Guangxi Basin, the ET/PET ratio was responsible for the LAI variations. There were also bidirectional causal relationships between LAI and the ET/PET ratio in some of these areas, indicating that vegetation was also a key factor affecting the water conditions.

3.3.5. Causal Link between Vegetation Greenness and LST

The Granger causality relationship between the LAI and LST is shown in Figure 20. No significant causality relationship was found in most of the regions in relation to the four main land cover types (Figure 20). In most of the low-latitude regions, such as YN and the Guangxi Basin, and significant negative correlation was observed between LAI and LST (Figure 15), and LST was a unidirectional cause of LAI variation. In higher latitude regions, such as the Hengduan Mountains and the Zoige Plateau in the west, HN, the border of SC, CQ, and GZ, LAI was a unidirectional cause of LST variation.

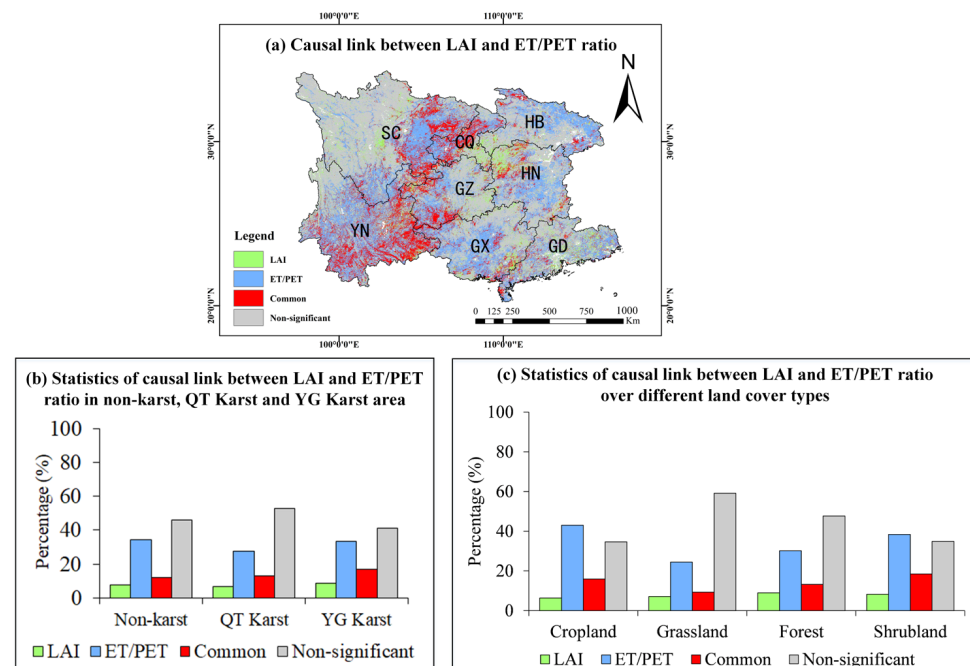


Figure 19. (a) Spatial patterns and statistics of the causality relationship between LAI and the ET/PET ratio over (b) different karst areas and (c) different land cover types in Southwest China. The red indicates bidirectional causal relationships between LAI and the ET/PET ratio; the green indicates that LAI is the unidirectional cause of the ET/PET ratio; the blue indicates that the ET/PET ratio is the unidirectional cause of LAI; and the grey shows that there are no significant causal links between LAI and the ET/PET ratio.

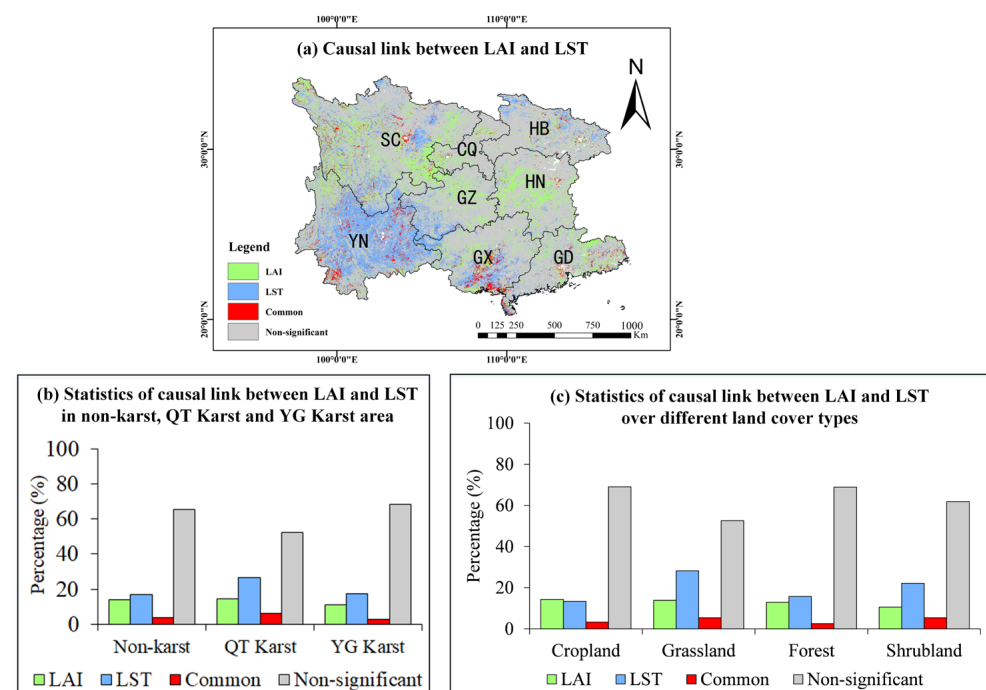


Figure 20. (a) Spatial patterns and statistics of the causality relationship between LAI and LST over (b) different karst areas and (c) different land cover types in Southwest China. The red indicates bidirectional causal relationships between LAI and LST; the blue indicates that LST is the unidirectional cause of LAI; the green indicates that LAI is the unidirectional cause of LST; the grey shows that there are no significant causal links between them.

4. Discussion

Most regions in southwestern China showed a greening trend during the period from 2001 to 2021. The implementation of some afforestation and conservation projects made a significant contribution to vegetation greening by converting some farmland and degraded land back to substantial natural land resources, such as forests, grassland, and shrubland [17,39,61]. For example, most of the lost grasslands were shown to have been converted to forests. In addition, the YG Karst area, which had more concentrated ecological engineering restoration projects reported in previous research [15,22], had a higher proportion of greening than non-karst or QT Karst area.

However, there might be a time lag between the implementation of ecological projects and vegetation growth, given that a large number of ecological projects to restore vegetation and alleviate rocky desertification have been implemented since the end of the 20th century [18,43]. Over the same period, climate change and human activities also had significant impacts on vegetation growth and the ecosystem as a whole [13]. During the period from 2001 to 2011, there were still some areas showing a decreasing trend in LAI. These areas were consistent with the areas and patterns of rocky desertification observed in previous studies [18]. While the greening trend was more obvious after 2012. In addition, small parts of areas show a significant and continuous trend of greening in both time periods (2001 to 2011 and 2012 to 2021) in all the four main land cover types of croplands, grasslands, shrublands, and forests (Figure 5). As most of the regions with a greening trend are undergoing a natural, creeping recovery process. The restoration of natural vegetation generally includes several successional stages, i.e., grass, grass-shrub, shrub, tree-shrub, and forest [22]. In this karst region, the transformation from a grassy community to a forest generally takes 30–50 years [22,65]. Considering that the area of reforestation was still limited [66], natural succession was dominant because of the geological background limitations [22].

The environmental factors that drive vegetation changes also showed a significant changing trend during the recent two decades, except for precipitation, which had no significant changing trend. The water conditions were shown to be improving in most of the regions of the study area. As TWS and ET/PET ratio showed an increasing trend since 2003, surface SM presented a decreasing trend during this period. However, the interactions between LAI and environmental factors varied with space. Specifically:

(1) In the YG Karst areas, including GZ, western GX, eastern YN, western CQ, etc., LAI is positively correlated with the water-related variables (except for central and eastern GZ), such as precipitation, TWS, and the ET/PET ratio. As vegetation growth in these areas are sensitive to water stress because of their particular geological structure featured as thin soil layers and weak water conservation capacity that hinders rainwater collection and storage and makes them more vulnerable to drought than other areas [18,67–69]. TWS and ET/PET ratio were shown to have unidirectional or bidirectional causal relationships with LAI. It indicates that vegetation changes may also significantly influence land-water conditions. That is, the restoration of vegetation by ecological engineering is conducive to the improvement of regional hydrological conditions, thereby further promoting the growth of vegetation in this area. Therefore, reforestation and vegetation restoration projects are suggested in these regions to improve the vegetation coverage as well as the ecological and meteorological environment.

(2) In the alpine regions located in the Northwest of YN and SC, including the Hengduan Mountains and the Zoige Plateau, most of the area did not have a significant vegetation greening trend, while in some areas, LST showed an obvious increasing trend. LAI was positively correlated with LST but negatively correlated with water-related factors, such as TWS and the ET/PET ratio. There was no significant causal relationship between LAI and ET/PET, with the exception of some valleys with low elevations. As the alpine regions have low mean annual temperatures (0–6 °C) and are energy-limited areas, temperature and solar radiation, rather than water stress, are the key limiting factors for vegetation growth [42]. Rising temperatures favor the growth of vegetation. Excessive precipitation

or prolonged rainy weather reduces solar radiation and temperature, both of which are detrimental to the growth of vegetation in this area. At the same time, rising temperatures cause snowmelt and a decrease in TWS. As the climate warming tendency leads to loss of meltwater through river runoff in this region [42,70]. In addition, LAI was found to be the cause of TWS and LST variations in this area. This indicates that vegetation changes can significantly affect water and energy balance in these high mountains. Therefore, natural succession instead of reforestation is suggested in this area, as direct reforestation might disrupt the water and energy balance in this region and accelerate the snowmelt and TWS loss.

(3) These southeastern regions, including HN, HB, GD, and eastern GX, are humid areas. TWS and ET/PET also showed an obvious increasing trend in most of the areas. Vegetation growth in these areas has a positive correlation with the ET/PET ratio but a significant negative correlation with surface SM and precipitation. As in the dry season, the improvement of water conditions is favorable to vegetation growth, while excessive precipitation in the rainy season usually causes waterlogging and flood disasters, considering the uneven seasonal distributions of precipitation in these regions [71,72]. Therefore, not only drought but also waterlogging should draw extensive attention, especially in the low-lying lands after heavy rainfall.

(4) In the SC Basin, the main grain producing area in Southwest China, LAI had a slight greening trend, and the water conditions were improved with increasing trends of the water-related variables, such as TWS and ET/PET ratio, during the recent two decades. LAI was positively correlated with the water-related variables: TWS, precipitation, and the ET/PET ratio. Most of the area in the SC Basin is covered by croplands. In addition, these variables were found to be the cause of LAI changes. LAI, in particular, was the cause of TWS and the ET/PET ratio in some regions of SC Basin. Considering the large water demand of crops, water is the key factor affecting vegetation growth in this region. The improvement of water conditions can promote crop production. In some regions, vegetation changes can also affect water conditions. However, SM showed a decreasing trend in this region, and LAI was found to be negatively correlated with SM. The SM data used in this study represents the surface water content, not necessarily the changing root-zone water conditions. Increasing the surface area of the SC Basin might increase the risk of waterlogging considering the relative lower elevation of the basin compared to the surrounding areas. Therefore, improving the root-zone water conditions through irrigation and surface water drainage would thus be suggested to promote the crop production in this region.

5. Conclusions

This study used remote sensing data to investigate the trends in vegetation growth and environmental factors, as well as their interactions, in southwestern China during the period from 2001 to 2021. Driven by climate change and human activities, such as ecological restoration projects, both vegetation and its water conditions have improved during the past two decades in most of the regions in southwestern China. A trend of vegetation greening was observed, with a weakening trend of rocky desertification and an increasing trend of vegetation growth during this period.

The alpine regions in the northwest of the study area are energy-limited areas, and vegetation growth and TWS changes there are sensitive to temperature. Vegetation changes were shown to be the cause of TWS and LST variations in many regions. Natural restoration measures, such as establishing nature reserves, returning grazing lands to grasslands, managing pests, etc., are suggested in this area to avoid strong disturbance in these areas. Direct ecological engineering implementation, such as reforestation, might strike the water- and energy-balance in this region and accelerate the snowmelt and TWS loss in these regions. The YG Karst area is water-limited due to the particular geological structure. It is vulnerable to drought, soil erosion, and rocky desertification. The improvement of regional hydrological conditions was shown to be beneficial to vegetation restoration there.

Meanwhile, vegetation greening has been shown to be the cause of increased TWS and an increase in the ET/PET ratio rising in many regions of the YG Karst area, that is to say, vegetation changes also positively feed back to the environmental factors through biogeophysical and biogeochemical processes. Ecological engineering projects that are beneficial to vegetation growth and soil and water conservation are suggested in this area, such as reforestation and soil erosion control. The vegetation growth in the SC Basin, HN, HB, GD, and eastern GX is sensitive to water stress, while these regions are vulnerable to waterlogging.

In summary, our study investigated the interactions between vegetation greenness and environmental factors and can help to improve the understanding of ecosystem management interventions, such as reforestation, natural vegetation restoration, and climate change mitigation. However, this study did not consider how the interactions may change in different seasons, and further in-depth studies are required.

Author Contributions: Conceptualization, H.L. (Haoxiang Li) and L.Z.; methodology, K.H. and H.L. (Haoxiang Li); validation, H.L. (Haoxiang Li); formal analysis, R.W., W.W., P.W. and J.S.; investigation, H.L. (Haichen Liu) and T.X.; resources, H.L. (Haoxiang Li); data curation, H.L. (Haichen Liu); writing—original draft preparation, K.H., R.W. and H.L. (Haoxiang Li); writing—review and editing, L.Z.; project administration, H.L. (Haoxiang Li) and L.Z. All authors have read and agreed to the published version of the manuscript.

Funding: This work was funded by the of National key Research and Development projects (No. 2019YFC0507502), Guangxi Key Research and Development Program (No. Guike AB19245040), Guangxi Key Research and Development Program (No. Guike AB19259015), Guangxi Key Research and Development Program (Guike AA20161004-1), Guangxi Key Research and Development Program (Guike AB21220044) and the Fundamental Research Funds for the Central Universities, Huazhong Agricultural University (No. 2662019QD054).

Institutional Review Board Statement: Not applicable.

Informed Consent Statement: Not applicable.

Data Availability Statement: Not applicable.

Acknowledgments: The authors would like to thank the editor and anonymous reviewers for their valuable comments to improve the quality of the paper.

Conflicts of Interest: The authors declare no conflict of interest.

References

- Piao, S.; Wang, X.; Park, T.; Chen, C.; Lian, X.; He, Y.; Bjerke, J.W.; Chen, A.; Ciais, P.; Tømmervik, H.; et al. Characteristics, drivers and feedbacks of global greening. *Nat. Rev. Earth Environ.* **2019**, *1*, 14–27. [[CrossRef](#)]
- Bonan, G.B.; Pollard, D.; Thompson, S.L. Effects of boreal forest vegetation on global climate. *Nature* **1992**, *359*, 716–718. [[CrossRef](#)]
- Xie, X.; He, B.; Guo, L.; Miao, C.; Zhang, Y. Detecting hotspots of interactions between vegetation greenness and terrestrial water storage using satellite observations. *Remote Sens. Environ.* **2019**, *231*, 111259. [[CrossRef](#)]
- Gyssels, G.; Poesen, J. The importance of plant root characteristics in controlling concentrated flow erosion rates. *Earth Surf. Processes Landf.* **2003**, *28*, 371–384. [[CrossRef](#)]
- Zhang, Y.; Xu, X.; Li, Z.; Liu, M.; Xu, C.; Zhang, R.; Luo, W. Effects of vegetation restoration on soil quality in degraded karst landscapes of southwest China. *Sci. Total Environ.* **2019**, *650*, 2657–2665. [[CrossRef](#)]
- Zeng, Z.; Piao, S.; Li, L.Z.X.; Zhou, L.; Ciais, P.; Wang, T.; Li, Y.; Lian, X.; Wood, E.F.; Friedlingstein, P.; et al. Climate mitigation from vegetation biophysical feedbacks during the past three decades. *Nat. Clim. Change* **2017**, *7*, 432–436. [[CrossRef](#)]
- Alkama, R.; Cescatti, A. Biophysical climate impacts of recent changes in global forest cover. *Science* **2016**, *351*, 600–604. [[CrossRef](#)]
- Descroix, L.; Viramontes, D.; Vauclin, M.; Gonzalez Barrios, J.L.; Esteves, M. Influence of soil surface features and vegetation on runoff and erosion in the Western Sierra Madre (Durango, Northwest Mexico). *CATENA* **2001**, *43*, 115–135. [[CrossRef](#)]
- Katul, G.G.; Oren, R.; Manzoni, S.; Higgins, C.; Parlange, M.B. Evapotranspiration: A process driving mass transport and energy exchange in the soil-plant-atmosphere-climate system. *Rev. Geophys.* **2012**, *50*, RG3002. [[CrossRef](#)]
- Istanbulluoglu, E.; Bras, R.L. On the dynamics of soil moisture, vegetation, and erosion: Implications of climate variability and change. *Water Resour. Res.* **2006**, *42*, W06418. [[CrossRef](#)]
- Chen, C.; Park, T.; Wang, X.; Piao, S.; Xu, B.; Chaturvedi, R.K.; Fuchs, R.; Brovkin, V.; Ciais, P.; Fensholt, R.; et al. China and India lead in greening of the world through land-use management. *Nat. Sustain.* **2019**, *2*, 122–129. [[CrossRef](#)] [[PubMed](#)]

12. Liu, H.; Jiao, F.; Yin, J.; Li, T.; Gong, H.; Wang, Z.; Lin, Z. Nonlinear relationship of vegetation greening with nature and human factors and its forecast—A case study of Southwest China. *Ecol. Indic.* **2020**, *111*, 106009. [[CrossRef](#)]
13. Peng, J.; Jiang, H.; Liu, Q.; Green, S.M.; Quine, T.A.; Liu, H.; Qiu, S.; Liu, Y.; Meersmans, J. Human activity vs. climate change: Distinguishing dominant drivers on LAI dynamics in karst region of southwest China. *Sci. Total Environ.* **2021**, *769*, 144297. [[CrossRef](#)] [[PubMed](#)]
14. He, Y.; Wang, L.; Niu, Z.; Nath, B. Vegetation recovery and recent degradation in different karst landforms of southwest China over the past two decades using GEE satellite archives. *Ecol. Inf.* **2022**, *68*, 101555. [[CrossRef](#)]
15. Tong, X.; Wang, K.; Yue, Y.; Brandt, M.; Liu, B.; Zhang, C.; Liao, C.; Fensholt, R. Quantifying the effectiveness of ecological restoration projects on long-term vegetation dynamics in the karst regions of Southwest China. *Int. J. Appl. Earth Obs. Geoinf.* **2017**, *54*, 105–113. [[CrossRef](#)]
16. Wang, K.; Zhang, C.; Chen, H.; Yue, Y.; Zhang, W.; Zhang, M.; Qi, X.; Fu, Z. Karst landscapes of China: Patterns, ecosystem processes and services. *Landsc. Ecol.* **2019**, *34*, 2743–2763. [[CrossRef](#)]
17. Wu, L.; Wang, S.; Bai, X.; Tian, Y.; Luo, G.; Wang, J.; Li, Q.; Chen, F.; Deng, Y.; Yang, Y.; et al. Climate change weakens the positive effect of human activities on karst vegetation productivity restoration in southern China. *Ecol. Indic.* **2020**, *115*, 106392. [[CrossRef](#)]
18. Qiao, Y.; Jiang, Y.; Zhang, C. Contribution of karst ecological restoration engineering to vegetation greening in southwest China during recent decade. *Ecol. Indic.* **2021**, *121*, 107081. [[CrossRef](#)]
19. Huang, Q.; Cai, Y. Mapping Karst Rock in Southwest China. *Mt. Res. Dev.* **2009**, *29*, 14–20. [[CrossRef](#)]
20. Li, S.; Ren, H.D.; Xue, L.; Chang, J.; Yao, X.H. Influence of bare rocks on surrounding soil moisture in the karst rocky desertification regions under drought conditions. *CATENA* **2014**, *116*, 157–162. [[CrossRef](#)]
21. Liu, Y.; Huang, X.; Yang, H.; Zhong, T. Environmental effects of land-use/cover change caused by urbanization and policies in Southwest China Karst area—A case study of Guiyang. *Habitat Int.* **2014**, *44*, 339–348. [[CrossRef](#)]
22. Qi, X.; Wang, K.; Zhang, C. Effectiveness of ecological restoration projects in a karst region of southwest China assessed using vegetation succession mapping. *Ecol. Eng.* **2013**, *54*, 245–253. [[CrossRef](#)]
23. Zhang, M.; Wang, K.; Liu, H.; Wang, J.; Zhang, C.; Yue, Y.; Qi, X. Spatio-Temporal Variation and Impact Factors for Vegetation Carbon Sequestration and Oxygen Production Based on Rocky Desertification Control in the Karst Region of Southwest China. *Remote Sens.* **2016**, *8*, 102. [[CrossRef](#)]
24. Tong, X.; Wang, K.; Brandt, M.; Yue, Y.; Liao, C.; Fensholt, R. Assessing Future Vegetation Trends and Restoration Prospects in the Karst Regions of Southwest China. *Remote Sens.* **2016**, *8*, 357. [[CrossRef](#)]
25. Yang, Y.; Long, D.; Guan, H.; Scanlon, B.R.; Simmons, C.T.; Jiang, L.; Xu, X. GRACE satellite observed hydrological controls on interannual and seasonal variability in surface greenness over mainland Australia. *J. Geophys. Res. Biogeosciences* **2014**, *119*, 2245–2260. [[CrossRef](#)]
26. Richey, A.S.; Thomas, B.F.; Lo, M.H.; Reager, J.T.; Famiglietti, J.S.; Voss, K.; Swenson, S.; Rodell, M. Quantifying renewable groundwater stress with GRACE. *Water Resour. Res.* **2015**, *51*, 5217–5238. [[CrossRef](#)] [[PubMed](#)]
27. Velicogna, I.G.A.; Kimball, J.S.; Kim, Y. Impact of changes in GRACE derived terrestrial water storage on vegetation growth in Eurasia. *Environ. Res. Lett.* **2015**, *10*, 124024. [[CrossRef](#)]
28. Felfelani, F.; Wada, Y.; Longuevergne, L.; Pokhrel, Y.N. Natural and human-induced terrestrial water storage change: A global analysis using hydrological models and GRACE. *J. Hydrol.* **2017**, *553*, 105–118. [[CrossRef](#)]
29. Wang, J.; Song, C.; Reager, J.T.; Yao, F.; Famiglietti, J.S.; Sheng, Y.; MacDonald, G.M.; Brun, F.; Schmied, H.M.; Marston, R.A.; et al. Recent global decline in endorheic basin water storages. *Nat. Geosci.* **2018**, *11*, 926–932. [[CrossRef](#)]
30. Chen, Y.; Velicogna, I.; Famiglietti, J.S.; Randerson, J.T. Satellite observations of terrestrial water storage provide early warning information about drought and fire season severity in the Amazon. *J. Geophys. Res. Biogeosci.* **2013**, *118*, 495–504. [[CrossRef](#)]
31. Long, D.; Scanlon, B.R.; Longuevergne, L.; Sun, A.Y.; Fernando, D.N.; Save, H. GRACE satellite monitoring of large depletion in water storage in response to the 2011 drought in Texas. *Geophys. Res. Lett.* **2013**, *40*, 3395–3401. [[CrossRef](#)]
32. Thomas, A.C.; Reager, J.T.; Famiglietti, J.S.; Rodell, M. A GRACE-based water storage deficit approach for hydrological drought characterization. *Geophys. Res. Lett.* **2014**, *41*, 1537–1545. [[CrossRef](#)]
33. Qu, S.; Wang, L.; Lin, A.; Zhu, H.; Yuan, M. What drives the vegetation restoration in Yangtze River basin, China: Climate change or anthropogenic factors? *Ecol. Indic.* **2018**, *90*, 438–450. [[CrossRef](#)]
34. Liu, H.; Zhang, M.; Lin, Z.; Xu, X. Spatial heterogeneity of the relationship between vegetation dynamics and climate change and their driving forces at multiple time scales in Southwest China. *Agric. For. Meteorol.* **2018**, *256*, 10–21. [[CrossRef](#)]
35. Ma, Y.; Zuo, L.; Gao, J.; Liu, Q.; Liu, L. The karst NDVI correlation with climate and its BAS-BP prediction based on multiple factors. *Ecol. Indic.* **2021**, *132*, 108254. [[CrossRef](#)]
36. Arora, V.K.; Montenegro, A. Small temperature benefits provided by realistic afforestation efforts. *Nat. Geosci.* **2011**, *4*, 514–518. [[CrossRef](#)]
37. Griscom, B.W.; Adams, J.; Ellis, P.W.; Houghton, R.A.; Lomax, G.; Miteva, D.A.; Schlesinger, W.H.; Shoch, D.; Siikamaki, J.V.; Smith, P.; et al. Natural climate solutions. *Proc. Natl. Acad. Sci. USA* **2017**, *114*, 11645–11650. [[CrossRef](#)]
38. Wang, J.; Wang, K.; Zhang, M.; Zhang, C. Impacts of climate change and human activities on vegetation cover in hilly southern China. *Ecol. Eng.* **2015**, *81*, 451–461. [[CrossRef](#)]
39. Tong, X.; Brandt, M.; Yue, Y.; Horion, S.; Wang, K.; Keersmaecker, W.D.; Tian, F.; Schurgers, G.; Xiao, X.; Luo, Y.; et al. Increased vegetation growth and carbon stock in China karst via ecological engineering. *Nat. Sustain.* **2018**, *1*, 44–50. [[CrossRef](#)]

40. Cai, H.; Yang, X.; Wang, K.; Xiao, L. Is Forest Restoration in the Southwest China Karst Promoted Mainly by Climate Change or Human-Induced Factors? *Remote Sens.* **2014**, *6*, 9895–9910. [[CrossRef](#)]
41. Ma, B.; Jing, J.; Liu, B.; Xu, Y.; Dou, S.; He, H. Quantitative assessment of the relative contributions of climate change and human activities to NPP changes in the Southwest Karst area of China. *Environ. Sci. Pollut. Res. Int.* **2022**, *29*, 80597–80611. [[CrossRef](#)] [[PubMed](#)]
42. Jiang, S.; Chen, X.; Smettem, K.; Wang, T. Climate and land use influences on changing spatiotemporal patterns of mountain vegetation cover in southwest China. *Ecol. Indic.* **2021**, *121*, 107193. [[CrossRef](#)]
43. Zhang, X.; Yue, Y.; Tong, X.; Wang, K.; Qi, X.; Deng, C.; Brandt, M. Eco-engineering controls vegetation trends in southwest China karst. *Sci. Total Environ.* **2021**, *770*, 145160. [[CrossRef](#)] [[PubMed](#)]
44. Piao, S.; Yin, G.; Tan, J.; Cheng, L.; Huang, M.; Li, Y.; Liu, R.; Mao, J.; Myneni, R.B.; Peng, S.; et al. Detection and attribution of vegetation greening trend in China over the last 30 years. *Glob. Change Biol.* **2015**, *21*, 1601–1609. [[CrossRef](#)] [[PubMed](#)]
45. Fan, Z.-X.; Bräuning, A.; Thomas, A.; Li, J.-B.; Cao, K.-F. Spatial and temporal temperature trends on the Yunnan Plateau (Southwest China) during 1961–2004. *Int. J. Climatol.* **2011**, *31*, 2078–2090. [[CrossRef](#)]
46. Watkins, M.M.; Wiese, D.N.; Yuan, D.-N.; Boening, C.; Landerer, F.W. Improved methods for observing Earth’s time variable mass distribution with GRACE using spherical cap mascons. *J. Geophys. Res. Solid Earth* **2015**, *120*, 2648–2671. [[CrossRef](#)]
47. Wiese, D.N.; Landerer, F.W.; Watkins, M.M. Quantifying and reducing leakage errors in the JPL RL05M GRACE mascon solution. *Water Resour. Res.* **2016**, *52*, 7490–7502. [[CrossRef](#)]
48. Landerer, F.W.; Flechtner, F.M.; Save, H.; Webb, F.H.; Bandikova, T.; Bertiger, W.I.; Bettadpur, S.V.; Byun, S.H.; Dahle, C.; Dobslaw, H.; et al. Extending the Global Mass Change Data Record: GRACE Follow-on Instrument and Science Data Performance. *Geophys. Res. Lett.* **2020**, *47*, e2020GL088306. [[CrossRef](#)]
49. Tapley, B.D.; Bettadpur, S.; Ries, J.C.; Thompson, P.F.; Watkins, M.M. GRACE measurements of mass variability in the Earth system. *Science* **2004**, *305*, 503–505. [[CrossRef](#)]
50. Andrew, R.; Guan, H.; Batelaan, O. Estimation of GRACE water storage components by temporal decomposition. *J. Hydrol.* **2017**, *552*, 341–350. [[CrossRef](#)]
51. Mu, Q.; Heinsch, F.A.; Zhao, M.; Running, S.W. Development of a global evapotranspiration algorithm based on MODIS and global meteorology data. *Remote Sens. Environ.* **2007**, *111*, 519–536. [[CrossRef](#)]
52. Wan, Z. New refinements and validation of the collection-6 MODIS land-surface temperature/emissivity product. *Remote Sens. Environ.* **2014**, *140*, 36–45. [[CrossRef](#)]
53. Song, P.; Zhang, Y.; Guo, J.; Shi, J.; Zhao, T.; Tong, B. A 1 km daily surface soil moisture dataset of enhanced coverage under all-weather conditions over China in 2003–2019. *Earth Syst. Sci. Data* **2022**, *14*, 2613–2637. [[CrossRef](#)]
54. Zhang, X.; Liu, L.; Wu, C.; Chen, X.; Gao, Y.; Xie, S.; Zhang, B. Development of a global 30 m impervious surface map using multisource and multitemporal remote sensing datasets with the Google Earth Engine platform. *Earth Syst. Sci. Data* **2020**, *12*, 1625–1648. [[CrossRef](#)]
55. Liu, L.; Zhang, X.; Gao, Y.; Chen, X.; Shuai, X.; Mi, J. Finer-Resolution Mapping of Global Land Cover: Recent Developments, Consistency Analysis, and Prospects. *J. Remote Sens.* **2021**, *2021*, 1–38. [[CrossRef](#)]
56. Zhang, X.; Liu, L.; Chen, X.; Gao, Y.; Xie, S.; Mi, J. GLC_FCS30: Global land-cover product with fine classification system at 30 m using time-series Landsat imagery. *Earth Syst. Sci. Data* **2021**, *13*, 2753–2776. [[CrossRef](#)]
57. Mann, H.B. Nonparametric tests against trend. *Econometrica* **1945**, 245–259. [[CrossRef](#)]
58. Granger, C.W.J. Investigating Causal Relations by Econometric Models and Cross-spectral Methods. *Econometrica* **1969**, *37*, 424–438. [[CrossRef](#)]
59. Green, J.K.; Konings, A.G.; Alemohammad, S.H.; Berry, J.; Entekhabi, D.; Kolassa, J.; Lee, J.E.; Gentile, P. Regionally strong feedbacks between the atmosphere and terrestrial biosphere. *Nat. Geosci.* **2017**, *10*, 410–414. [[CrossRef](#)]
60. Sugihara, G.; May, R.; Ye, H.; Hsieh, C.H.; Deyle, E.; Fogarty, M.; Munch, S. Detecting causality in complex ecosystems. *Science* **2012**, *338*, 496–500. [[CrossRef](#)]
61. Yang, Y.; Wang, S.; Bai, X.; Tan, Q.; Li, Q.; Wu, L.; Tian, S.; Hu, Z.; Li, C.; Deng, Y. Factors Affecting Long-Term Trends in Global NDVI. *Forests* **2019**, *10*, 372. [[CrossRef](#)]
62. Wang, W.; Wang, W.-j.; Li, J.-s.; Wu, H.; Xu, C.; Liu, T. The Impact of Sustained Drought on Vegetation Ecosystem in Southwest China Based on Remote Sensing. *Procedia Environ. Sci.* **2010**, *2*, 1679–1691. [[CrossRef](#)]
63. Zhao, X.; Wei, H.; Liang, S.; Zhou, T.; He, B.; Tang, B.; Wu, D. Responses of Natural Vegetation to Different Stages of Extreme Drought during 2009–2010 in Southwestern China. *Remote Sens.* **2015**, *7*, 14039–14054. [[CrossRef](#)]
64. Shi, Y.; Gao, X.; Wu, J.; Giorgi, F. Changes in snow cover over China in the 21st century as simulated by a high resolution regional climate model. *Environ. Res. Lett.* **2011**, *6*, 045401. [[CrossRef](#)]
65. He, X.-Y.; Wang, K.-L.; Zhang, W.; Chen, Z.-H.; Zhu, Y.-G.; Chen, H.-S. Positive correlation between soil bacterial metabolic and plant species diversity and bacterial and fungal diversity in a vegetation succession on Karst. *Plant Soil* **2008**, *307*, 123–134. [[CrossRef](#)]
66. Wang, X.; Li, S.; Huang, S.; Cui, Y.; Fu, H.; Li, T.; Zhao, W.; Yang, X. Pinus massoniana population dynamics: Driving species diversity during the pioneer stage of ecological restoration. *Glob. Ecol. Conserv.* **2021**, *27*, e01593. [[CrossRef](#)]
67. Lian, Y.; You, G.J.-Y.; Lin, K.; Jiang, Z.; Zhang, C.; Qin, X. Characteristics of climate change in southwest China karst region and their potential environmental impacts. *Environ. Earth Sci.* **2014**, *74*, 937–944. [[CrossRef](#)]

68. Wan, L.; Zhou, J.; Guo, H.; Cui, M.; Liu, Y. Trend of water resource amount, drought frequency, and agricultural exposure to water stresses in the karst regions of South China. *Nat. Hazards* **2015**, *80*, 23–42. [[CrossRef](#)]
69. Zhou, Q.; Luo, Y.; Zhou, X.; Cai, M.; Zhao, C. Response of vegetation to water balance conditions at different time scales across the karst area of southwestern China-A remote sensing approach. *Sci. Total Environ.* **2018**, *645*, 460–470. [[CrossRef](#)]
70. Deng, H.; Pepin, N.C.; Liu, Q.; Chen, Y. Understanding the spatial differences in terrestrial water storage variations in the Tibetan Plateau from 2002 to 2016. *Clim. Change* **2018**, *151*, 379–393. [[CrossRef](#)]
71. Zhang, H.; Wu, C.H.; Chen, W.J.; Huang, G.R. Assessing the Impact of Climate Change on the Waterlogging Risk in Coastal Cities: A Case Study of Guangzhou, South China. *J. Hydrometeorol.* **2017**, *18*, 1549–1562. [[CrossRef](#)]
72. Lyu, H.-M.; Xu, Y.-S.; Cheng, W.-C.; Arulrajah, A. Flooding Hazards across Southern China and Prospective Sustainability Measures. *Sustainability* **2018**, *10*, 1682. [[CrossRef](#)]